# Synthesis of $Cu_2O$/ZnO/kaolinite composite for the degradation of methylene blue under visible light

By: Paulos Asefa Fufa

A thesis submitted to

The Department of Materials Science and Engineering

School of Mechanical, Chemical and Materials Engineering

Presented in Partial Fulfillment of the Requirement for the Degree of Master

in Materials Science and Engineering

Office of Graduate Studies

Adama Science and Technology University

Adama

July, 2020 G.C

# Synthesis of $Cu_2O$/ZnO/kaolinite composite for the degradation of methylene blue under visible light

By: Paulos Asefa Fufa

Advsor name: Dr. Osman Ahmed (Ph.D)

Co-adivisor name: Dr. Gebissa Bekele (Ph.D)

A thesis submitted to

The Department of Materials Science and Engineering

School of Mechanical, Chemical and Materials Engineering

Presented in Partial Fulfillment of the Requirement for the Degree of Master

in Materials Science and Engineering

Office of Graduate Studies

Adama Science and Technology University

Adama

July, 2020 G.C

## Approval of Board of Examiners

We, the undersigned, members of the Board of Examiners of the final open defense by Paulos Asefa Fufa, ID No: PGR/18412/11, have read and evaluated his thesis Entitled: "**Synthesis of $Cu_2O$/ZnO/kaolinite composite for the degradation of methylene blue under visible light"**, and examined the candidate. This is, therefore, to certify that the thesis has been accepted in partial fulfillment of the requirement for the Degree of masters of Science in Materials Science and Engineering.

| | | |
|---|---|---|
| --- | --- | --- |
| Advisor | Signature | Date |
| --- | --- | --- |
| External Examiner | Signature | Date |
| --- | --- | --- |
| Internal Examiner | Signature | Date |

## Advisors Approval Sheet

To: Materials Science and Engineering Department

Subject: Thesis Submission

This is to certify that the M.Sc thesis entitled "Synthesis of $Cu_2O$/ZnO/Kaolinite nanocomposite for the decolorization of methylene blue under visible light", Submitted in partial fulfillment of the requirements for the degree of Masters of Science in Materials and Engineering, to the post graduate programs of the Department of Materials Science and Engineering, and has been carried out by Paulos Asefa Fufa ID No: PGR/18412/11, under our supervision. Therefore, we recommend that the student has fulfilled the requirement and hence hereby he can submit the thesis to the department.

| | | |
|---|---|---|
| Advisor | Signature | Date |
| Co-Advisor | Signature | Date |

## Declaration

I hereby declare that this M.Sc thesis is my original work and has not been submitted in candidature for a degree in any other university, and all sources of materials used for this thesis have been duly acknowledged.

| ---------- | ---------- | ---------- |
|---|---|---|
| Student name | Signature | Date |

Approved by Advisors:

| ---------- | ---------- | ---------- |
|---|---|---|
| Advisor | Signature | Date |
| ---------- | ---------- | ---------- |
| Co-advisor | Signature | Date |

# Synthesis of $Cu_2O$/ZnO/kaolinite composite for the degradation of methylene blue under visible light

By: Paulos Asefa Fufa

A thesis submitted to

The Department of Materials Science and Engineering

School of Mechanical, Chemical and Materials Engineering

Presented in Partial Fulfillment of the Requirement for the Degree of Masters

in Materials Science and Engineering

Office of Graduate Studies

Adama Science and Technology University

Adama

July, 2020

# Synthesis of $Cu_2O$/ZnO/kaolinite composite for the degradation of methylene blue under visible light

By: Paulos Asefa Fufa

Advsor name: Dr. Osman Ahmed (Ph.D.)

Co-adivisor name: Dr. Gebissa Bekele (Ph.D.)

A thesis submitted to

The Department of Materials Science and Engineering

School of Mechanical, Chemical and Materials Engineering

Presented in Partial Fulfillment of the Requirement for the Degree of Masters in Materials Science and Engineering

Office of Graduate Studies

Adama Science and Technology University

Adama

July, 2020 GC

## Approval of Board of Examiners

We, the undersigned, members of the Board of Examiners of the final open defense by Paulos Asefa have read and evaluated his thesis Entitled: "**Synthesis of $Cu_2O$/ZnO/kaolinite composite for the degradation of methylene blue under visible light"**, and examined the candidate. This is, therefore, to certify that the thesis has been accepted in partial fulfillment of the requirement for the Degree of masters of Science in Materials Science and Engineering

| | | |
|---|---|---|
| Advisor | Signature | Date |
| External Examiner | Signature | Date |
| Interna Examiner | Signateure | Date |
| Chair Person | Signature | Date |

## Advisors Approval Sheet

To: Materials Science and Engineering Department

Subject: Thesis Submission

This is to certify that the M.Sc thesis entitled "Synthesis of $Cu_2O$/ZnO/kaolinite composite for the degradation of methylene blue under visible light", Submitted in partial fulfilment of the requirements for the degree of Masters of Science in Materials Science and Engineering, to the graduate programs of the Department of Materials Science and Engineering, and has been carried out by Paulos Asefa Fufa ID No: PGR/18412/11, under our supervision. Therefore, we recommend that the student has fulfilled the requirement and hence hereby he can submit the thesis to the department.

| | | |
|---|---|---|
| Advisor | Signature | Date |
| Co-Advisor | Signature | Date |

## Declaration

I hereby declare that this M.Sc thesis is my original work and has not been submitted in candidature for a degree in any other University, and all sources of materials used for this thesis have been duly acknowledged.

---------- ---------- ----------

Student name Signature Date

Approved by Advisors:

---------- ---------- ----------

Advisor Signature Date

---------- ---------- ----------

Co-advisor Signature Date

# ACKNOWLEDGEMENT

First Almighty to my God, for everything done for me. Next, I would like to show my deepest gratitude to Dr. Osman Ahmed, and Dr. Gebissa Bekele, for their constructive criticism, suggesting valuable information, inspiring guidance and strong outstanding with me through this research work.

Am deeply grateful to my beloved family, and especially Ms. Kalale Ephrem for their supporting and motivational speech that made me strong without doubtful.

Also, I would like to extend my deepest gratitude to all staffs of Materials Science and Engineering especially Mr. Demeke Tesfaye for running XRD, DTG and UV-vis DRS of my samples, Dr. Dinsefa Mensur for running SEM samples, his advice and patience starting from the beginning, Mr. Andualem Merga for his advice and facilitating materials through my thesis work. Dr. Temesgan Debelo and Dr. Fiqadu Aga for their advice and motivational Speech they shared for me. Outside of my department staffs, I would like to say thank you to Mr. Bundi from Chemical Engineering Staffs, Mr. Guta from Chemistry staffs, Mr. Iticha from Biology Staffs for their support by providing me Materials.

Lastly, but not the least I would like to thanks **Adama Science and Technology University** for providing me this Masters Scholarship and all funded for this thesis work as well as Materials Science and Engineering Department. This research project is funded by Adama Science and Technology University granted under grant number ASTU/MS-R/127/19.

# TABLE OF CONTENTS

# LIST OF FIGURES

# LIST OF TABLES

# List of Acronyms and Abbreviations

AAS ..... .....Atomic Absorption spectroscope

DTA..... ..... .....Differential Thermal Analysis

TGA.....Thermal Gravimetric Analysis

EDS ..... .....Energy Dispersive Spectroscopy

SEM.....Scanning Electron Spectroscopy

XRD.....X-ray Diffractometry

FTIR..... Fourier transformed Infrared Spectroscopy

UV-vis DRS.....Ultra Violet visible Diffuse reflectance spectroscopy

C.....$Cu_2O$

Z.....ZnO

K.....kaolinite

ZK.....ZnO/Kaolinite

CK.....$Cu_2O$/Kaolinite

5CZK.....5 % of $Cu_2O$/ZnO/Kaolinite

10CZK.....10 % of $Cu_2O$/ZnO/Kaolinite

15CZK.....15 % of $Cu_2O$/ZnO/Kaolinite

20CZK.....20 % of $Cu_2O$/ZnO/Kaolinite

D.....particle size diameter

**Abstract**

*Different chemicals used during the industrial processing such as textiles, leathers, papers, and cosmetics are released to the environment and cause severe problems. These released chemicals contain tremendous amounts of toxic organic pollutants, inorganic pollutants and heavy metals. Due to their effects on the environment, they should be controlled effectively and economically to survive human life and the environment through photodegradation process by using photocatalyst materials.*

*Herein, we design to synthesize a novel $Cu_2O$/ZnO/kaolinite composite by co-precipitation method. The synthesized composite catalysts are termed as 5CZK, 10CZK, 15CZK, and 20CZK which represents 5 %, 10 %, 15 % and 20 % of $Cu_2O$, respectively, on ZnO/kaolinite composite. The X-ray Diffraction (XRD), Differential Thermal Analysis (DTA), Thermogravimetric Analysi (TGA), Atomic Absorption Spectroscopy (AAS), Fourier Transform Infrared Spectroscopy (FTIR), Scanning Electron Microscopy (SEM) and UV-Visible Diffuse Reflectance Spectroscopy (UV-visible DRS ) were used to characterize the as-synthesized catalysts. Moreover, the photocatalytic degradation of methylene blue dye was selected as a target organic pollutants and evaluated under visible light irradiation. The highest performance for the degradation of 125 mL (10 ppm) methylene blue dye was achieved by 25 mg of 10CZK catalyst within 105 min. The enhanced degradation of 10CZK composite may be due to the synergetic effects and light-responsive under visible light by Coupling p-type $Cu_2O$ with n-type ZnO which in turn reduce the electron-hole pair recombination through the formation of heterojunction. Hence, in our study, the optimum ternary catalyst was achieved by loading 10 % of $Cu_2O$ on the ZnO/kaolinite composite with appropriate conditions.*

*On the other hand, the preferable conditions for MB dye degradation in acidic, neutral and basic media were also checked. The complete degradation of MB dye was achieved in basic media within 30 min and almost suppressed with decreased pH to acidic media. This shows that the cationic MB dye prefer basic sites for adsorption and strong attraction force between the negatively charged kaolinite and cationic dye in basic media. Besides, the stability and reusability of the catalyst were also checked. The catalyst shows good stability and reusability until $5^{th}$ cyle. This reveals that the synthesized composite catalyst also could be applicable for environmental remediation and industrial applications with low cost.*

# CHAPTER 1
# INTRODUCTION

## 1.1. Background of the Study

Water is fundamental for life and about 70% of the earth region is secured with water. However, only 2.5 % is fresh water which is used for human life [1]. Due to this scarcity of fresh water, water recycling and reusing may offer the chance to extend the water resources. Particularly, the rapid growth in population, industrialization, agricultural activities, geological and environmental changes, etc. are among the factors, that increase the number of poisons and released into water, air and soil system [2]. Because of this, industrial wastes should be controlled effectively and economically to survive human life and the environment.

Nowadays different methods could be used for wastewater treatment. Among the technologies used, electrocoagulation/flocculation [3-6], adsorption [7-9], separation [10] , membrane process [11], disinfection [12], and photocatalysis [13-15] have been used recently. However, some of the technologies need huge infrastructure and consumes large amounts of energy. In addition to this, the formation of secondary pollution, containing health-threatening bacteria and soluble refractory organic species which cannot easily be removed from contaminated water are also the disadvantages [16, 17]. Particularly, conventional wastewater treatment methods cannot degrade the majority of the pollutants. Hence, it is important to choose cost-effective and powerful methods for the decontamination of dye. Wastewaters have received increasing attention over the past decade. Among the techniques, advanced oxidation processes (AOPs) which are a relatively new and promising set of techniques have been developed and employed for dye contaminated industrial effluent treatment.

The researchers also give attention to find low cost and low energy consumption technology called photocatalysis, which has great potential and high efficiency to remove organic and inorganic pollutants. Photocatalysis is also a green technology process that uses solar light to convert photonic energy into valuable chemical energy. Particularly, the heterogeneous photocatalytic reduction and oxidation is a green and candidate technology in the fields of energy, environment, and chemistry which mainly rely on semiconductor materials and solar energy [16, 18].

Among semiconductor materials, titanium dioxide ($TiO_2$), zinc oxide (ZnO), iron (III) oxide ($Fe_2O_3$), zirconia ($ZrO_2$), vanadium (V) oxide ($V_2O_5$), niobium pentoxide ( $Nb_2O_5$) and tungsten trioxide ($WO_3$) have been widely studied and used as a photocatalyst in the field of environmental waste management system [19]. Moreover, semiconductors such as $TiO_2$ and ZnO are widely used and applicable metal oxide due to their unique properties such as chemical stability, photo-catalytic characteristics, durability, relative nontoxicity, strong oxidizing, low cost, biocompatibility, antimicrobial activities, and high redox potential and environmentally friendly [20-23]. However, they have limited application due to their wide bandgap energy ($TiO_2$ (Eg ≈ 3.32), ZnO (Eg ≈ 3.37 eV)) and only absorbs photons in the UV region with wavelengths approximately 380 nm. ZnO exhibit high quantum efficiency compared to the $TiO_2$ due to its electron mobility (200-300 $cm^{-1}V^{-1}s^{-1}$) which is higher than that of $TiO_2$ (0.1 – 4.0 $Cm^{-1}V^{-1}$ $s^{-1}$) [24, 25]. Hence, ZnO compound can absorb a higher fraction of UV spectrum and shows higher photocatalytic performance for the degradation of organic pollutants than $TiO_2$ [26-31]. It is known that only about 5 % of the solar light incident on the earth's surfaces are occupied by UV region [20]. However, about 45 % of the energy belongs to visible light. Hence, to increase the photocatalytic activity of ZnO, it is important to extend the UV region to the visible region by narrowing band gap of ZnO and increasing electron-hole pair separation using different methods. For instance, doping with non-metals [32, 33], transitional metal, [34, 35] and coupling with other heterogeneous semiconductor materials [36, 37].

Moreover, porosity is also another issue in the photocatalytic activities of the materials. To increase the porosity, it is important to synthesize metal oxides and clay composites. The recovering of small-sized photocatalyst after treatment is also another challenge which is technically obstacle. The reactivity and toxicity of nanoparticles on the environment and animals [38], plants [38], and humans [39] are also the current issues. Hence, such drawbacks can be solved by using inorganic matrices to anchored ZnO nanoparticles and other small-sized nano photocatalysts on the surface of clay without affecting their unique properties [40].

Therefore, clay minerals are one of the matrices used for this purpose due to its unique properties such as its natural abundance on the earth's surface, high porosity, high surface area, thermal stability, and its biocompatibility to the environment. Nowadays, clays are mainly used as supports of ZnO based photocatalyst. Due to their high surface area and large pore volume [41, 42], clays absorb organic substances on their external surfaces and within their interlaminar spaces. Among them, kaolinite is one of the natural clay minerals that mainly used for cosmetics and healing as well as inspected to be used for the water treatment, is a promised material that enables particles to anchor on its surface.

Kaolinite is considered as 1:1 phyllosilicates layered clay and/or is two-dimensional layered Aluminosilicate riched with enough hydroxyl radicals group on its surface that participates in interfacial reactions [43]. Kaolinite contains octahedral aluminium hydroxide sheet (either gibbsite ($Al(OH)_3$) or brucite ($Mg(OH)_2$) stacked on each other) and tetrahedral silicate sheet [44-46]. The fast and efficient adsorption- degradation process is observed due to the large adsorption sites present on the surfaces of kaolinite, and its micron dimension makes it ease for rapid and high efficient recovering [43, 47]. Inserting semiconductor photocatalyst in clay not only leads to the formation of more active surface sites to enhance the efficiency but also used to inhibit the formations of large aggregations of photoactive particles that reduce the efficiency of photocatalyst [43, 48].

There are many reports on metal oxides and kaolinite composites for different application. Such as Kutláková *et al.* [40] synthesized eco-friendly kaolinite/ZnO nanocomposite with high photocatalytic activity $TiO_2$/Kaolinite [43], ZnO/Kaolinite [40], g-$C_3N_4$/Kaolinite[49], co-loading of $TiO_2$ and $C_3N_4$ on kaolinite [50], BiOCl/g-$C_3N_4$/kaolinite [51] have been reported. These composites exhibited enhanced photocatalytic efficiency compared to their pure particles without combined with kaolinite. Misra *et al.* [52] also synthesized Doped ZnO nanoparticles impregnated on Kaolinite (Clay) of a reusable nanocomposite for photocatalytic disinfection of multidrug-resistant Enterobacter sp. under visible light.

It is also important to obtain ultra-high efficiency of ZnO/Kaolinite composite. Designing of the ternary photocatalyst through *p-n* hetero-junction is also another method to enhance the photocatalytic activities. Among the *p*-type semiconductor, copper-based materials are widely applicable due to their low bandgap, low cost, non-toxic nature and abundance [53]. $Cu_2O$ is a *p*-type semiconductor characterized by low bandgap about 2.1 eV

which enables as it shows strong absorption of visible light [54]. Therefore, coupling *n*-type ZnO with *p*-type $Cu_2O$ exhibit enhanced photocatalytic activities in the visible region. On the other hand, single ZnO or $Cu_2O$ shows decreased efficiency of photocatalytic activities due to their high recombination of photogenerated electron-hole pairs [54, 55]. Hence, these recombination rates are can be decreased by the formation of *p-n* type hetero-junctions called ZnO-$Cu_2O$ hetero-junction. In addition to this, $Cu_2O$ has the potential to absorb molecular oxygen and then $O_2$ reacts with water and photo-generated electrons to generate $H_2O_2$ and OH radicals with strong oxidizing properties, finally oxidizing organic substances to smaller molecules such as $CO_2$ and $H_2O$ [56-58]. Many researchers synthesized ZnO/$Cu_2O$ hetero-junctions with improved photocatalytic efficiency. For example, Xu *et al.* [59] ZnO/$Cu_2O$ compound photocatalyst and application in treating organic dyes. They found that the ZnO/$Cu_2O$ compound exhibited enhanced photocatalytic activities compared to their individual due to the reduced electron-hole recombination. However, it is still important to increase the photocatalytic activities of ZnO/$Cu_2O$ by anchoring it on the materials having high absorption capacity like kaolinite. In additions, stability and recoverability of this composite can be obtained by using kaolinite as a matrices which is the main challanges in catalysis today. Due to this reason, our target is to design ZnO/$Cu_2O$ anchored on the natural kaolinite which can be considered as alternative and efficient photocatalyst materials to get high photocatalytic activities.

However, there is no report on Ethiopian kaolin and metal oxide nanocomposite for wastewater treatments even if the potential of kaolin as support for photocatalyst is widely studied in the world. So far the potential of Ethiopian kaolin clay has been reported as the candidate materials for synthesizing of Zeolite [60], electrical porcelain insulator [61], and mainly for ceramics production [60] rather than for the photocatalyst applications.

Herein, we report $Cu_2O$/ZnO/Kaolinite nanocomposite for the wastewater treatment using facile synthesis methods. The synthesized materials were characterized by AAS, XRD, SEM, TGA, DTA, FTIR, and UV-Visible DR Spectroscopy etc, and finally, the photocatalytic activity of the synthesized samples was also evaluated. The synthesized samples expected to have high efficiency for the degradation of methylene blue. This efficiency might be due to the high surface area, high porosity and the formation of hetero-junctions that reduce electron-hole recombination rate of the synthesized composite. Also, the stability and reusability of the catalyst were also checked.

## 1.2. Statement of the problems

The fast economic growths of many countries are relying on the industry, because Industry is termed as "engine" for economic growth. Among these industries, the textile industry is one of the manufacturing industries that strongly add values to economic growth. However, the textile industry needs large amounts of chemicals and waters to complete at various stages during production, which at the end releases many effluents that affect the environment and human health [62]. In developing countries, during the textile industry operating wastewater is not recyclable due to the economic issues.

Herein Ethiopia, there are several manufacturing industries including textile industries that release a tremendous amount of organic pollutants like organic dyes. These organic dyes can cause serious health problems and environmental pollution. To alleviate such kind of problems, many works had been reported. Among them, the cost-effective and environmentally benign method is named as photocatalysis. The candidate materials for photocatalyst are semiconductor metal oxide.

Widely, ZnO semiconductor is used as photocatalytic activities; however, it exhibits low surface area, high carrier recombination rate due to its wide bandgap (Eg ≈ 3.37eV), function only under UV region and non-recoverable. To overcome these limitations, we proposed to use kaolin clay and the formation of hetero-junctions $Cu_2O$/ZnO composite for the following reasons; (1) kaolin clay will be used for two purposes; first, as a support for the metal oxide nanocomposite so that $Cu_2O$/ ZnO nanocomposite can be recyclable. The second case is for the absorption of organic pollutants within its interlaminar spaces. (2) $Cu_2O$ selected due to its low bandgap, low cost, non-toxic nature, abundance, and shows strong absorption of the visible light. Due to aforementioned reasons, it will be expected that photocatalyst $Cu_2O$/ZnO nanocomposite anchored on the kaolin clay has less carrier recombination due to *n-p* junction formation of $Cu_2O$/ZnO, high surface area owing to interspaces of kaolin clay. As a result of these, the proposed photocatalyst material can exhibit adsorption – degradation process of organic pollutants. Therefore, the synthesized composite expected to exhibit high performance for the methylene blue degradation due to its synergetic effects.

## 1.3. General objective

Synthesis of $Cu_2O$/ZnO/kaolinite composite for the degradation of methylene blue under visible light.

## 1.4. Specific objectives

- ✓ To characterize chemical compositions, crystal structures, thermal analysis and surface morphology of locally available raw kaolin clay.
- ✓ To synthesize ZnO, $Cu_2O$, $Cu_2O$/ZnO, kaolinite phase only, ZnO/kaolinite, $Cu_2O$/kaolinite, and $Cu_2O$/ ZnO/kaolinite composite photocatalyst.
- ✓ To characterize the synthesized samples and evaluations of photocatalytic activities of prepared catalyst on methylene blue degradation.
- ✓ To study pH effect, stability, and reusability of the synthesized catalyst.
- ✓ To identify Reactive Oxygen Species (ROS) participated in the photocatalytic activity.

## 1.5. Scope of the study

This thesis research was delimited to the synthesize of ternary $Cu_2O$/ZnO/kaolinite composite photocatalyst based locally available kaolin clay for degradations methylene blue at laboratory scale.

## 1.6. Significance of the study

The significance of this study is to develop and characterize the potential of the locally available raw materials supported metal oxide semiconductor composite for the applications of wastewater treatment. To propose the easy, cost-effective and high-efficiency methods for the industries to treat wastewater contaminated by organic and inorganic pollutants released during the industrial processing. Besides this, saving the lives of humans, plants, and animals which are affected by the contaminated wastewater will also be the benefit obtained from this research. In addition to this, the demand for kaolin clay will increase significantly and offer great advantages for society who lives around these raw materials.

# CHAPTER 2
# LITERATURE REVIEW

## 2.1. Water pollution

Water contaminations are caused as a result of human activities including industrial, mining and agricultural activities, etc, to survive their life on earth. Even if these activities are beneficiary to human life, they also bring health risk diseases such as diarrhoea, cholera, dysentery, hepatitis is the results of water contamination [63]. Nowadays, about 80 % of the worldwide population is faced with water death and two million deaths annually due to water contamination [64]. Among these agent explained above the main sources of water pollution, it has been reported that the organic compounds released from the industrial dyes and textiles dyes during the processes are the major source of water pollution. Also, Heavy metals released during the industrial processes are other major sources of water contamination. Hence, it is important to alleviate such problems. In this chapter, different methods of wastewater treatments will be discussed briefly. Moreover, the photocatalysis process, key points about kaolin clay will be discussed here briefly. Finally, a summary of kaolin based photocatalyst will be summarized in tabular form.

## 2.2. Methods of wastewater treatment

So far, many researchers have been attempted to search methods of wastewater treatment technology which is efficient and effective. Mainly these technologies treatments are focused on physiochemical, electrochemical, biological and advanced oxidation process as shown in Figure 2.1. However, complete mineralization of organic pollutants is obtained only through the photocatalysis process which is considered under advanced oxidation technology [65].

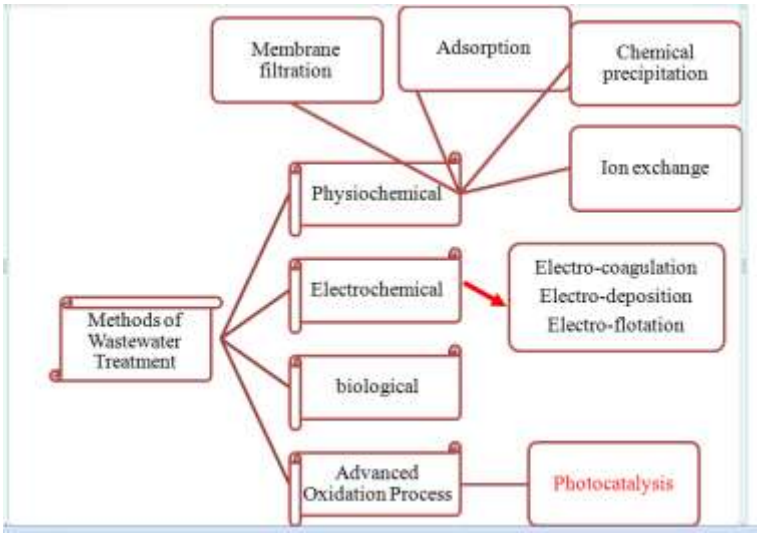


Figure 2.1 Methods of Wastewater Treatment

## 2.3. Heterogeneous photocatalyst

Photocatalysis is a promising technology for solving energy use, environmental remedi ation and chemical synthesis issues, such as hydrogen production through water splitting and organic pollutants degradation. Photocatalysts can be defined as a substance that increases the rate of a reaction by absorbing light and remain the same at the end of the reaction [66].

Photocatalysts can be categorized into Homogeneous and Heterogeneous photocatalytic process. In the homogeneous photocatalytic process, the hydroxyl ions are generated by the metal complex ions with higher oxidation states under the photon and thermal situation. It used as a catalyst with transition metal complexes such as iron, copper, chromium, etc, In this case, organic pollutants can be reacted with the hydroxyl ions generated and can lead to the removal of toxic substances. But, when compared to the heterogeneous, the degradation of organic pollutants from wastewater is mainly done by heterogeneous photo-catalytic process due to its ability to degrade organic pollutants that cannot be easily controlled [67].

With increasing their applications in environmental remediation and solar energy conversion, the importance of the semiconductor heterogeneous photocatalyst also increased [66]. This process posses several advantages such as complete mineralization, low cost, no waste disposal problems and environmentally friendly compared to other methods [68]. ZnO, $TiO_2$, $CeO_2$, $SnO_2$, $WO_2$, $Fe_2O_3$, CdSe, etc are semiconductors materials with their unique electronic structure properties characterized by their empty valence band and filled conduction band, charge transport characteristics and excited states of a lifetime.

Among heterogeneous photocatalyst, ZnO has been studied due to its characteristics low price, its excellent stability, enormous facile preparation methods, it's exceptional electrical, optical, environmental friendless [21, 22, 69-71]. Because of these properties and its high photocatalytic activity, this research deals with ZnO based metal oxide photocatalysts.

### 2.4. Mechanism of photocatalysis

The mechanism of photocatalysis is similar to the principles of the photochemical reaction that takes place in semiconductor but with some complexity. In a semiconductor, the chemical reaction could take place due to the electron transferred from the valence band to the conduction band. Whereas in the photocatalytic oxidation process, when the light with energy equal or greater than the bandgap energy of the semiconductors photocatalyst hit the surface of the catalyst, the electrons will jump from the valence band to the conduction band by leaving the holes in the valence band. The holes left in the valence band have strong ability to oxidize donor molecules and react with the water molecules to generate free radical species called hydroxyl radicals. These generated hydroxyl radicals have the strong oxidizing potential to degrade the organic pollutants and then leads to the complete mineralization of organic pollutants. Whereas, the electrons excited to the conduction band reacts with the dissolved oxygen to produces Oxygen activated species such as superoxide anions. To give the desired products the holes and electrons should undergo Redox process with any species which might be adsorbed on the surface of semiconductor [72-75]. Photocatalytic responses are caused by photo-catalyst like $TiO_2$ absorbing photon with greater energy than its bandgap as shown in Figure 2.2 [76].

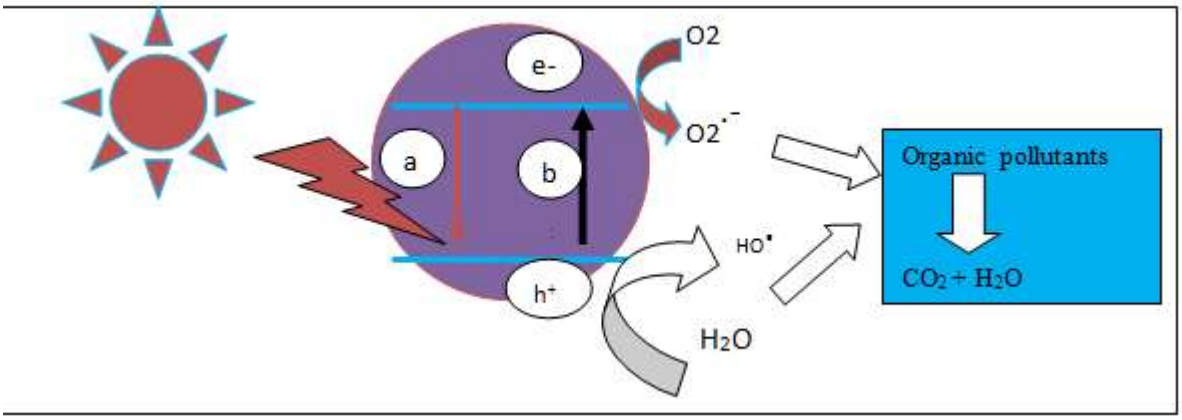


Figure 2.2 Mechanism of Photocatalysis (a) Recombination, (b) Excitation

## 2.4.1. Oxidation mechanism

The absorbed water on the surface of the photocatalyst is oxidized by the holes formed as the result of electron excitation from the valence band to the conduction band due to the applied light energy, to yield Hydroxyl radicals (which have the power to decompose organic pollutants). This hydroxyl radical reacts with the organic pollutants present in the dyes. Then, the organic pollutants are completely mineralized to Carbon dioxide and water. During the process, if Oxygen is involved, the oxygen molecules with intermediate radicals in an organic compound can form radical chain reactions and sometimes they consume oxygen. By following this manner finally, they lead to complete mineralization of organic pollutants as shown in Figure 2.3 [67, 74].

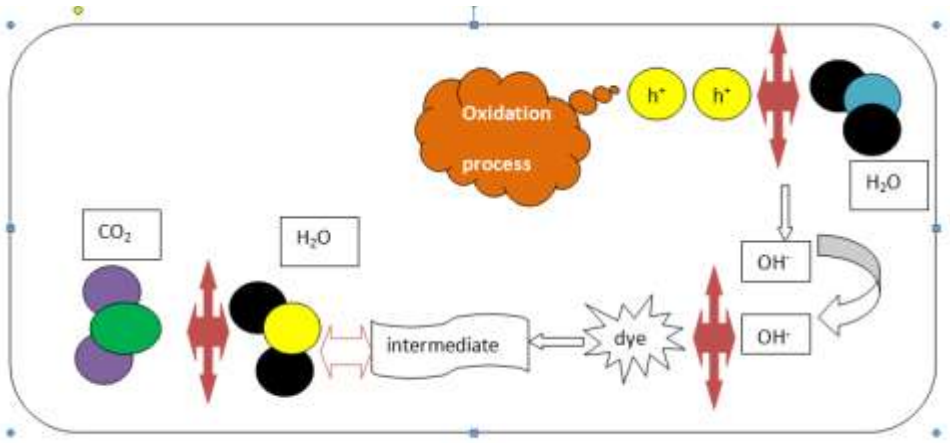


Figure 2.3 Schematic representation mechanism for oxidation

## 2.4.2. Reduction mechanism

The electrons excited from the valence band to the conduction band can undergo further reduction process as shown in Figure 2.4. Since oxygen is easily reducible substances, the reduction of oxygen is used as the best choice for the generation of hydrogen. Superoxide anions are formed when the dissolved oxygen species react with the electrons excited to the conduction band without recombination. These superoxide anions formed are attached to the intermediate products in Oxidative reaction to form peroxide or hydrogen peroxide and finally altered to water as observed from Figure 2.4 [67, 74].

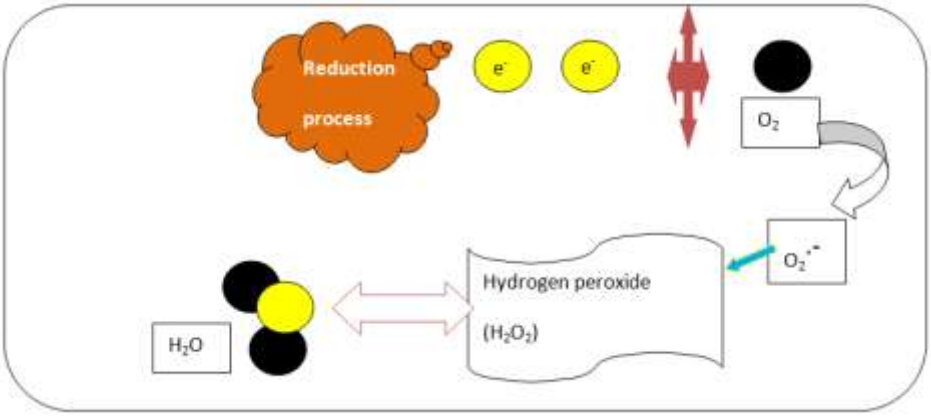


Figure 2.4 Schematic representing of reduction mechanism

## 2.5. Photocatalytic semiconductors

Metal oxides are the most candidate semiconductor materials for photocatalysis. Metal oxides such as $TiO_2$, ZnO, $WO_3$, $Fe_2O_3$, $SnO_2$, $ZrO_2$, $V_2O_5$, $Ag_2O$, $AgCrO_4$, etc have been mostly studied for photocatalytic application [68, 73, 77]. In 1972, Fujishima and Honda first used $TiO_2$ semiconductor to photochemically decompose water [78]. Due to its long term stability, relative non-toxicity, strong oxidizing, low cost, biocompatibility and abundance, the applications of $TiO_2$ have been studied as semiconductor photo-catalyst [79, 80]. $TiO_2$ is characterized by three main crystal structures. Namely, Anatase (tetragonal), Rutile (tetragonal) , $TiO_2$ (B) and Brookite (Orthorhombic). Among them, Anatase and rutile crystal structures are the most widely applicable structures of $TiO_2$ in photocatalytic applications. However, due to its low electron mobility and high electron-hole recombination in rutile, Anatase shows higher photocatalytic actives than rutile [81, 82]. Despite this fact, $TiO_2$ has a large bandgap that limits its applications in UV region.

ZnO is also another semiconductor material that used in photocatalytic applications due to its unique properties such as, optoelectronic properties, good chemical stability, abundance, non-toxicity, low cost, high redox potential and environmentally friendly [21-23]. It's also characterized by large band-gap (3.37 eV) and a high exciton binding energy (60 meV) [83]. ZnO exhibits high quantum efficiency compared to the $TiO_2$ due to its electron mobility (200-300 $Cm^{-1}V^{-1}s^{-1}$) which is higher than that of $TiO_2$ (0.1 – 4.0 $Cm^{-1}V^{-1}$ $s^{-1}$) [24, 25]. Hence, this compound can absorb a higher fraction of the UV spectrum and shows higher photocatalytic performance for the degradation of organic pollutants than $TiO_2$ [26-31]. ZnO's VB position is lower than that of $TiO_2$'s VB; as such, ZnO's hydroxyl radical

oxidation potential is greater than that of $TiO_2$'s hydroxyl radical [84]. Therefore, the photocatalytic efficiency of ZnO in degrading pollutants is generally greater than that of $TiO_2$ [85]. However, the larger bandgap enables ZnO to absorb UV light only (4 % solar spectrum) but not visible light (43 % solar spectrum) [86]. Hence, this thesis concerned with the improvement of ZnO limitations .

## 2.6. Parameters affect photocatalysis

The photocatalytic characteristics and efficiencies are affected by the photocatalyst's surface structures, including surface area, porosity, catalyst loading, defects, pH, initial pollutant concentration, reaction temperature, calcination temperature, light intensity, agitation speed, etc. Altering each parameter will affect the efficiency of photocatalytic degradation. These parameters are discussed here one by one.

### 1. Catalyst Loading

The degradation rate of the organic compound is affected by the catalyst concentration which depends on the initial concentration of pollutants and the amount of solution present in the sample. Generally, increasing the catalyst loading the degradation rate of the organic compound also increases [87]. This due to the formation of more hydroxyl species ($OH^{\cdot}$) and oxygen radicals ( $O_2^{\cdot -}$ ) with an increased amount of catalyst concentrations which contains more active catalyst sites. However, after the optimum value further increasing of catalyst concentration leads to a decrease in photocatalytic activity due to decreased light penetration depth into the solution and diminish light scattering ability [88, 89]. Hence, the catalyst concentration in any solution and degradation rate is directly proportional to each other until the optimum concentration. S.Chakrarti et al.[90] reported the effect of different ZnO loading on the degradation rate of the dye. As they investigated, the percent of dye degradation increased from 47 to 74 % with increased catalyst loading from 0.2 to 1.0 g in 400 mL after 2 hours. However, a further increase in catalyst loading had no significant impacts on percentage degrade. Finally, they proved that the maximum degradation rate for Eosin Y was 1 g in 400 mL of solution. Hence, the amount of catalyst loading has a great impact on the degradation rates of organic pollutants.

## 2. Effects of Shape, Size, Surface Area and Crystal Structures of Catalyst

Many researchers investigate the morphology dependence of photocatalytic activities. For example, different photocatalytic characteristics of nanostructures of ZnO have been investigated. Such as, nanofilms [91], nanospheres [92], nanorods [93], nanocubes [94], and nanofibers [95]. Among them, the most promising nanofibers provide high aspect ratio and specified flow pattern for improved photocatalytic property [96, 97]. $TiO_2$ is characterized by triphase such as anatase, rutile, and brookite. Among them, the anatase phase is the most accepted phase for photocatalyst compared to the others [98, 99]. This is due to its stability, the position of the conduction band, the higher degree of hydroxylation and absorption power [100, 101]. Materials at nano-level exhibit new unique properties such as large surface area, high aspect ratio compared to the bulk one. Nano-sized $TiO_2$ shows higher photocatalytic activities than bulk $TiO_2$ due to its small size, large surface area, large surface volume ratio [99]. Since the reaction takes place on the surface of the catalyst it is important to know the effect of surface on the efficiency of photocatalytic activities.

## 3. pH Effect

The pH of the solution is a vital factor in the photocatalytic reactions, as it is made a clear explanation of the photocatalyst's proper bonds on the surface loading. Kottam *et al.* reported the change in pH can affect the efficiency of photocatalytic degradation of organic pollutants [102-104].

However, interpretation of the impact of pH on the effectiveness of photo-degradation of colors is very challenging task due to it is linked to various variables such as surface ionization, acid-base properties of surface particles and reactant colors and their products [88]. Neppolian *et al.* reported that the percentage degradation of reactive Blue 4 was not significantly affected by acidic pH, whereas the inhibitory impact was more pronounced in the alkaline range (pH 11-13) [105]. This has been studied by considering different conditions of pH value to observe photocatalytic degradation of $TiO_2$ catalyst for Reactive Blue. The result shows the reduced degradation efficiency of Reactive Blue in acidic solution ($pH<5$) due to the elevated concentrations of proton that retards the photodegradation of the dye. However, the existence of hydroxyl ions defuses the acidic end products produced by the photo-degradation response in alkaline medium ($pH>10$). An unexpected decrease in degradation in the alkaline range (pH 11-13) is due to hydroxyl

radicals ($OH^{\cdot}$) is found to be quickly scavenged and does not respond with coloring [88, 105]. Generally, pH value has a great impact on degradation efficiency of photo-catalytic activities.

**4. Calcination Temperature**

Calcination is heat treatment process and one of the parameters that affect the photocatalytic activities. This process can also affect the micro-structural properties as well as the photocatalytic activities. Zhang *et al.* group studied the effect of calcination on the photo-catalytic properties of nano-sized $TiO_2$ powders by considering different temperatures [99]. The observed result shows that the photocatalytic degradation of phenol is higher at 400 ℃ than dried at 110 ℃. However, after 600 ℃ of calcination temperatures, the photocatalytic degradation efficiency of phenol solution decreased significantly. This is due to larger size observed at higher temperatures which result in high recombination rates of electrons and holes photogenerated. He *et al.* reported the impacts of calcination temperatures on the photocatalytic properties of ZnO by pyrolysis method [106]. They summarize the effect of calcination temperatures are may rely on morphological, surface and optical properties of ZnO samples. Generally, the effects of calcination temperatures on photocatalytic activities have been studied by many researchers [107-109].

**5. Light Intensity**

Light intensity is also one of the parameters that affect the photocatalytic activities of degradation efficiency. For example, ZnO exhibited strong absorption edge around 381 nm due to its large band gap energy which restricts the applications of ZnO only under UV radiation. Hanh *et al.* reported that the removal of mono-crotophos pesticide by ZnO prepared under visible light has not been observed [110]. However, when doped with Copper that is Cu-doped ZnO shows only small amounts of degradation efficiency. This result demonstrates that the degradation observed is due to the lowered band-gap of ZnO by dopping with Copper, thus shift the wavelength of light sources. This in turn increases the generation of electrons and holes pairs that enhance the photocatalytic activities. The more light intensive irradiation is the more photocatalytic reaction due to the increased electron-hole pairs separation activity [111]. Benabbou *et al.* investigated the impacts of light intensity on degradation rate of the $TiO_2$ catalyst by considering different light intensity as follows; the light intensity increased from 0.48 MW/cm$^2$ to 3.85 MW/cm$^2$ so does reaction rates [112]. As well as time for degradation is increased from 60 to 90 minutes with decreased light intensity

from 3.85 to 0.48 MW/cm$^2$. Therefore, the photocatalysis processes strongly depend on the light intensity and high efficiency will be observed at a higher intensity or under visible light.

## 2.7. Improvement of photocatalyst efficiency

Among the metal oxide semiconductors used for photocatalytic activities, $TiO_2$, ZnO and $CeO_2$ are the most studied by many researchers due to their unique properties [73]. For instance, $TiO_2$ is considered as better photocatalyst compared to other metal oxides due to its high stability, high quantum efficiency, non-toxicity, low cost, wide spread availability and noncorrosive properties [113, 114]. ZnO and $CeO_2$ catalyst exhibit the same bandgap around 3.24 eV with $TiO_2$ however they show favored photocatalytic activity due to their high absorption properties, higher efficiency of generation, mobility, separation of photoinduced electrons and holes [115, 116]. Unsuccessfully, both $TiO_2$ and ZnO show their performance only under UV rather than in visible region due to their larger bandgap. These limitations can lead to fast electrons- holes recombination, which in turn lower the photocatalytic efficiency. Since the sunlight devotes about 46 % Visible light, 4 – 5 % Ultraviolet light and 47 % Infrared radiations, $TiO_2$ and ZnO semiconductors active only in absorbing 4 – 5 % of sunlight. Hence, they are failure to cause large potential of solar for photocatalytic activities. In order to overcome these limitations many approaches have been used to cause them absorb photons of lower energy as well [117]. These approaches are doping with metals and non-metals, coupling with different metal and metal oxides, etc, mainly used to reduce electrons – holes recombination which enhance photocatalytic activities of semiconductor catalyst and discussed hereafter one by one.

## 2.7.1. Bandgap modifications by non-metal doping

### A. Nitrogen Doping

The failure of both ZnO and $TiO_2$ in visible light response has been improved by nitrogen doping [117]. Due to its equivalent atomic size with oxygen, small ionization, metastable center formation, high stability and low-cost Nitrogen doping is more preferable than other non-metals [118]. Yang *et al.* synthesized N-doped $TiO_2$ by solvothermal method [119]. They observed that the higher photocatalytic activities of N-doped $TiO_2$ due its improved broad absorption in the visible light region for the degradation of organic dyes (Methylene Blue and Methylene Orange) [119]. With nitrogen doping, the band gap of $TiO_2$ changed from 3.2 eV to 2.5 eV.

### B. Sulfur Doping

Sulfur doping is one of the techniques that have been used to modify band-gap of semiconductor photocatalyst materials as it shows their photocatalytic activities in visible region. Hsu *et al.*[120] explained the photocatalytic activities of S-doped ZnO are higher than undoped ZnO due to the incorporated sulfur. The additions of sulfur leads to higher absorption of light by tuning the band-gap of ZnO and promote its activity under visible region. The degradation of methylene blue by using S-doped ZnO catalyst exhibits enhanced visible light activities and improved antibacterial activities than pure ZnO [121].

### C. Carbon doping

Non-metal doping such as Carbon can improve the photocatalytic activities of semiconductor catalyst ( eg. ZnO, $TiO_2$ ) by increasing absorption of light and reducing electrons-holes recombination. Haibo *et al.* reported that the prepared Carbon doped ZnO shows a narrowed band gap with expanded visible region wavelength up to 800 nm and so enhanced efficiency of photocatalytic activities [122]. The enhanced visible-light photocatalytic efficiency of Carbon-doped $TiO_2$ for the degradations of organic pollutants such as methylene blue, rhodamine, and p-nitrophenol also has been investigated [123-125].

**D. F and I Doping**

The photocatalytic activities of ZnO and $TiO_2$ catalysts can also be improved by F and I doping similar to C, S, N, anionic doping. Liu et al.[126] reported that F-doped $TiO_2$ exhibits increased photocatalytic activities in visible region due to the Oxygen vacancy created. The degradation of P-chlorophenol of organic pollutants by I-doped $TiO_2$ obtained is 95.7 % under visible light irradiation which is higher than obtained P25 (5.5 %) catalyst [20]. This is due to the modified band-gap and electronic properties of $TiO_2$ by iodine doping. The iodine doped $TiO_2$ shows the decreased band-gap and exhibit enhanced photocatalytic activities [127].

## 2.7.2. Bandgap modifications by metal doping.

Semiconductor Oxide properties can be modified by doping with transition metals, rare earth metals, alkali metals, and noble metals [128-132]. Metals doped ZnO can extended visible light response of ZnO and improves the efficiency of it. For example, optical, electrical, photocatalytic activities, gas sensitivity and magnetic properties of ZnO have been modified by replacing copper into ZnO lattice [133, 134]. The prepared Cu-doped ZnO exhibited high photocatalytic activities due to the reduced electron-hole recombination rate on the surface of it [135]. Alam *et al.*[136] investigated the rare earth metals ( La, Nd, Sm, and Dy)- doped ZnO by facile sol-gel methods. They found that metal-doped ZnO showed enhanced photocatalytic activities for the degradations of methylene Blue and rhodamine B due to the reduced electron-hole recombination of Rare earth doped ZnO. Generally, the band-gap of semiconductor oxides can be modified by doping of metal transitions or rare earth metals. These doped semiconductor oxide reflects the enhanced photodegradation efficiency of organic dyes.

## 2.*7.3.* Hetero-structure semiconductors

The designing of hetero-structure semiconductors by a combination of two or more nano-crystalline materials makes it more helpful in photocatalysis, water splitting, microelectronics, and others. The reason why designing of hetero-structure semiconductors are so important is; (1) coupling large band-gap semiconductors with a lower band-gaps leads to broaden photo-response, (2) it reduces electron-hole recombination by transferring electrons into the lower-lying conduction band of the large band-gap semiconductors. This can be achieved by coupling semiconductor/metal, semiconductor/semiconductor, and etc

[137]. Composites can diminish the large bandgaps of semiconductors so enhance the photocatalytic activities.

## 2.8. Synthesis methods of metal oxides nanocomposite

Various methods have been investigated for the synthesis routes of metal oxide nanoparticles. Among them, the five synthesis routes that have been used mostly are considered here.

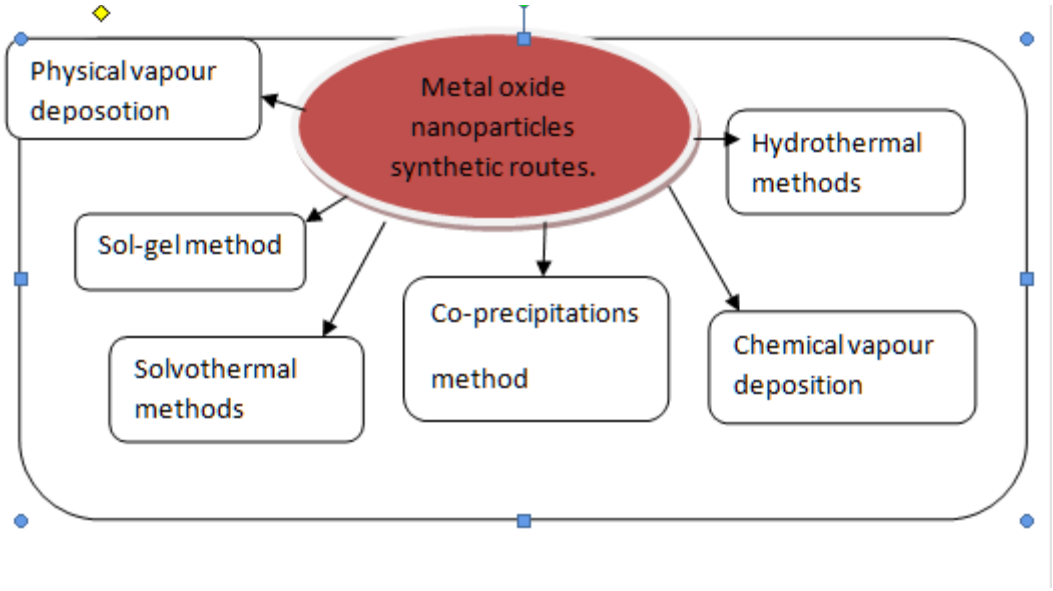


Figure 2.5 Some Synthesis Methods of Metal Semiconductor Nanoparticles

### A. Coprecipitation

Coprecipitation methods provide some advantages such as simple and rapid preparation, composition and particle size is easy to control, the particle surface state and overall homogeneity can be modified using different possibilities, low temperature, energy-efficient and etc. In spite of this it exhibit some drawbacks such as not applicable to uncharged species, trace impurities may also get precipitated with the product, time-consuming, batch to batch reproducibility problems and doesn't effectively work if the reactants have very different precipitation rates [138].

### B. Chemical Vapor Deposition

Chemical vapor deposition (CVD) is the method in which films of materials are deposited on the surfaces of the substrate from the vapor phase through the decompositions of chemicals as a result of thermal energy [139]. It is a chemical method in which high quality,

high performance of solid materials are produced at the end and mainly used in the semiconductor industry to the production of thin films. Generally, water or substrate is exposed to one or more volatile precursors that react and/or decompose on the substrate surface to deposit the desired product. In addition the volatile by-products are also produced frequently which are finally removed by gas flow through the reaction chamber [138].

**C. Hydrothermal or Solvothermal Method**

A hydrothermal or solvothermal method is a technique that mainly used to synthesize nanomaterials with controlled morphology in which the reaction takes place in closed vessels under high temperature and pressure conditions. The reactants are placed into an autoclave filled with water or organic solvents to carry out the reaction. When the solvent used is water the techniques is termed as hydrothermal whereas if the solvent used is alcohol or nonaqueous it is called solvothermal method [138].

**D. Sol-gel**

Sol-gel is one of the well-stablished synthetic methods for preparing novel metal oxide particles as well as blended composite of oxide. Metal oxide formation includes various successive stages as follows; the metal precursor originally undergoes fast hydrolysis to generate metal hydroxide solution. Then subsequently undergoes condensation steps to form gel. The acquired gel subsequently undergoes a drying process and the resulting item is easily transformed to Xerogel or Aerogel based on the drying method. Based on the nature of the solvent used, sol-gel can be categorized into aqueous and non-aqueous sol-gel processes. If the solvent used is water, the process is called aqueous sol-gel process. While the organic solvent is used as a reaction medium it is called a non-aqueous sol-gel process [140].

## 2.9. Clay and clay minerals

The word clay relates to a naturally occurring material consisting of fine-grained (with grain size less than 2 $\mu m$ ) minerals, which usually plastic with adequate water content and will harden with either dried or fired. Whereas, the word " clay mineral" relates to minerals from the phyllosilicates and minerals that give plasticity to clay and harden when either dried or fired [141]. Based on their structure and composition, clay and clay minerals are applicable in many areas such as industries, engineering, construction and etc, [142]. Pure clays do not occur in nature; they contain mixtures of different clay and associated minerals [143]. Among the most common clay minerals such as bentonite, montmorillonite, attapulgite, mica,

sericite, hydrotalcite, fluoromica, hectorite, and saponite, only kaolin clay minerals with a chemical composition $Al_2Si_2O_5(OH)_4$ is the most commercially available clay minerals.

### 2.9.1. Kaolin group

The kaolin groups minerals such as kaolinite, dickite, nickrite, halloysite polymorphs contain dioctahedral 1:1 layer structures with the chemical compositions of $Al_2Si_2O_5(OH)_4$. Among these polytypes of kaolin, kaolinite is the most abundant. Kaolinite which is known as China clay after named for the locality of Kao-Ling in Kiangsi province that mined from $11^{th}$ century till 1964 and is 1:1 phyllosilicate formed when the silicon tetrahedral sheets and aluminum octahedral sheets are super positioned. The adjacent layers are held together by hydrogen bonds and weak van der Waals force [144]. Kaolinite is a natural clay minerals which is typically two-dimensional aluminum silicate layered and enriched with abundant hydroxyl groups on the surface that efficiently participate in any chemical reaction as well as ion transfer or exchange procedures [145].

Kaolinite is widely applicable industrial raw materials such as paper coating and filling, oil, ceramics, paint, cracking catalyst, cements, wastewater treatment, rubber, and pharmaceutical industries [141, 144]. The improvement of photocatalytic efficiency by kaolinite has been proven by many researchers due its important surface properties and high absorption capacity [146]. In addition to these properties its low cost, abundance, thermal resistance, and chemical stability leads kaolinite as it serves as catalyst support such as $TiO_2$ [49].

Wang *et al* [147]. investigated the enhanced photocatalytic efficiency of the $TiO_2$ by using kaolinite as a support. The result reflects that the synthesized $TiO_2$/kaolinite composite calcined at 200℃ exhibit high photocatalytic activities because of its smaller crystalline size, the abundant surface oxygen vacancies and defects and reduced electron-hole pair recombinations of anatase $TiO_2$. Similarly Sun *et al.*[49] teported the photocatalytic activities of Kaolinite/g-$C_3N_4$ composite were enhanced under light. Based on the research studied so far we can conclude that the potential of kaolinite as a support for catalysts to enhance the efficiency of photocatalytic activities. Since natural kaolinite minerals contain elements such as Fe, Ti, Mn, Mg and Cr, and impure phases like quartz, anatase and illite, the surface modifications of kaolinite is important. Chemical properties of kaolinite may be affected by these impurities and also surface properties of kaolinite [144].

## 2.9.2. Surface modifications of clay minerals

Surface modifications/functionalizing can leads to the achievement of specific properties that play a great role in environmental applications. Some of the techniques such as heat treatment, acid treatment, and base treatments are the most common for the modifications of the kaolinite surface [148]. However, the treatment of clays with alkaline has been much less studied but may be good for the preparation of Zeolite from the clay [149]. Therefore. only the heat treatment is discussed here for the aim of this research.

### 2.3.2.1. Heat treatment

Kaolin clay consists of high amount of kaolinite. When heated at some temperature it undergoes phase change. During heat treatment the dehydroxylation of kaolinite takes place and Metakaolinite ( amorphous phase) is formed as the following reaction equation 1 [150].

$$Al_2O_3.2SiO_2.2H_2O\ (s) \rightarrow Al_2O_3.2SiO_2\ (s) + 2H_2O\ (g) \quad (1)$$

Kaolinite = Metakaolinite + water

Also Xu et al.[151] reported the phase transformation of kaolinite at a temperature greater than or equal to 400 and 1000 ℃ according to the following equations (2) (3):

$$Al_2Si_2O_5(OH)_4 \rightarrow Al_2SiO_7 + 2H_2O \qquad T \geq 400\ ℃ \quad (2)$$

$$3(Al_2O_3.SiO_2) \rightarrow 3Al_2O_3.\ 2SiO_2 + SiO_2 \qquad T \geq 1000\ ℃ \quad (3)$$

The tetrahedral sheets formed by Si-O bonds are not altered in Metakaolinite. However, due to the dehydroxylation of Al-OH groups, the Octahedral sheets produced by Al-O bonds are significantly altered and rearranged into less organized tetrahedral patterns that can lead to the decided reaction ability and production of new bonds [152]. Under high temperature firing the kaolinite is directly changed mullite phase. which is major crystalline products. Above 980 ℃ the excess silica is formed in the form of impurity called quartz and changed to the amorphous silica when heated above 1200 ℃. Upon increasing temperature, this amorphous silica crystallizes to cristobalite and this cristobalite returned to the amorphous phase when heated above 1500 ℃ [151].

## 2.10. Summery of kaolinite based composite and their application

The summery of kaolinite based composite photocatalysts are listed in the table 2.1.

Table 2.1 Summary of kaolinite based composite with their applications.

| **Photocatalyst** | **Synthesis method** | **Applications** | **References** |
|---|---|---|---|
| Silver nanoparticles/kaolinite | | - | [153] |
| kaolinite/$TiO_2$ composite | Hydrolysis methods | Methylene orange degradations. | [147] |
| kaolinite/nano $TiO_2$ composite | - | Antibacterial activity | [154] |
| ZnO/kaoline nanocomposite | Thermal decomposition | Antibacterial activity | [155] |
| kaolinite/g-$C_3N_4$ | Mechanochemical method | Degradations of RhB under visible irradiations | [49] |
| kaolinite/ZnO nanocomposite | Hydrothermal | Degradation of AO7 | [40] |
| ZnO/kaolinite composite | Calcination of $Na_2Zn_3(CO_3)_4.2H_2O$ | Degradations of Acid orange 7 (AO7) | [156] |
| kaolinite/$TiO_2$ composite | Hydrolysis of titanyl sulfate | Degradations of acid Orange 7 (AO7) | [157] |
| kaolinite – titania composite | Sol-gel | Degradation of methylene Blue | [158] |
| kaolinite/$TiO_2$ nanocomposite | Sol-gel | Degradation of methylene blue and methylene Orange II | [159] |
| Pd hybridizing ZnO/kaolinite | ------- | Methylene blue degradation | [160] |

| | | | |
|---|---|---|---|
| Fe-doped ZnO/kaolinite | Co-precipitation | photocatalytic disinfection of multidrug-resistant *Enterobacter* sp. under visible light | [52] |
| BiOCl/g-$C_3N_4$/ kaolinite composite | Self-assembly | Degradations rhodamine | [51] |
| g-$C_3N_4$ / $TiO_2$ /Kaolinite composite | Solgel | Degradations of ciprofloxacin | [161] |
| $Cu_2O$/ZnO/kaolinite composite | Co-precipitation | Methylene blue degradation | This work |

Table 2.1. Shows the summery of kaolinite based composite with their applications. No one has reported on $Cu_2O$/ZnO/kaolinite composite which is the main goal of this thesis. Hopefully, this research is aimed to investigate novel $Cu_2O$/ZnO/Kaolinite composite for the degradation of organic pollutants released to the water during the industrial process. Specifically, methylene blue is considered for our target.

# CHAPTER 3
# MATERIALS AND METHODS

### 3.1. Chemicals and reagents

Bombowha clay (Kaolin) raw materials selected for this study was collected from the Tabor Ceramics Factory which is found in Hawassa, Ethiopia. The chemicals and reagents were analytical grade and used without further purification. $ZnCl_2$ (LOBA CHEMIE, 97%), $Cu(NO_3)_2.3H_2O$ (Sigma Aldrich, 99%) , Glucose, NaOH ( Turkey, AR Pellet Assay; 99.8%), Ethanol (Wasse PHARMA PLC., 96-99%), Isopropyl alcohol (AR–$C_3H_8O$ Ranchem Industry, Turkey), $AgNO_3$ (LOBA CHEMI), and disodium ethylene diamine-tetraacetate (EDTA-2Na) were used in this experiment

## 3.2. Experimental procedures

### 3.2.1. Purifications of kaolin

The kaolin clay was purified as follows: 40 g of kaolin clay was dissolved in 150 mL of distilled water under continuous stirring for four days at room temperature. The obtained mixtures were aged for three days and on the third day the upper liquid is decanted. Then, the higher density which was settled at the bottom is added to the cylinder of 1000 mL and subsequently, filled with distilled water and, shaked for a minute and allowed to settle. Based on stokes law clay particles settles with velocity of 902 $D^2$ mm/sec ( where D is the diameter of clay particles ) and the distance on the cylinder was measured. After measured, the lower density suspension was decanted to the beaker and filtered by Whatman number one filter paper. Finally, the filtered solution was dried in an oven at 110 ℃ overnight. For comparison purpose, a raw clay was used. Both samples are characterized by XRD. The purified one was kept for further synthesis.

### 3.2.2. Synthesis of ZnO and ZnO/kaolinite composite.

ZnO/kaolinite composite was synthesized by keeping the molar ratio of $Zn^{2+}$ : $OH^-$ being 1:5 and the mass ratio of kaolin to ZnO 1:1 ( 50%wt:50%wt) as reported by K. Mamulová Kutláková *et.al* [156]. In a particular procedure, 0.5 g of kaolin clay was dissolved in 50 mL distilled water and sonicated for 30 min. After sonication, 0.836 g of Zinc Chloride dissolved in 25 mL of distilled water was added dropwise to the clay suspension under stirring. Then, 25 mL (0.44 g ) of sodium hydroxide was added to the mixture and

allowed to react for 5 hr with continuous stirring. The resulting sample was washed,, dried at 100 °C for 12 hr, and finally calcined at 600 °C for 1 hr. The synthesized samples were kept for further experiment. ZnO was synthesized without kaolinite for comparison purpose.

### 3.2.3. Synthesis of $Cu_2O$/ZnO/kaolinite composite

To synthesize $Cu_2O$/ZnO/kaolinite composite (20CZK); 0.2 g of the as-synthesized ZnO/kaolinite composite was dissolved in 30 mL of distilled water and sonicated at 40 ℃ for 30 minute. After sonication, 20% of $Cu_2O$ (0.21 g of copper precursor,16 mL) was added to the suspension. Then, 0.9792 g of sodium hydroxide (16 mL) and 0.42 g (3 mL) of glucose (reducing agent) were added after 30 minutes. The mixture was continuously stirred for 1 hr and aged for 24 hr. subsequently, the upper solution was decanted and the settled solid was centrifuged three times by distilled waster, one time by alcohol. Finally, dried at 60 ℃ for 12 hr. The rest samples ( i.e 15CZK, 10CZK and 5CZK) were synthesized with the same procedures and the 15CZK, 10CZK and 5CZK represents 15%, 10%, and 5% of $Cu_2O$ loaded on the ZnO/Kaolinite, respectively. For comparison, similar procedures were applied for $Cu_2O$/ZnO, and $Cu_2O$.

## 3.3. Characterization techniques

Phase analysis of the samples were characterized by X-ray Diffractometry (XRD) ((Shi-madzu x-ray diffractometer 7000, Japan), using $CuK\alpha_1$ radiation ( $\lambda$ = 1.5418Å) generated by accelerated voltage of 40 kV and filament current 30 mA. Thermal stability of the sample was analyzed by Differential Thermal Gravometric (DTG) (Shimadzu DTG-60H, Japan), operating under inert atmosphere condition, the sample was heated from room temperature up to 1000 ℃ at a rate of 10 ℃/min in a platinum cup and other empty platinum cup was used as a control. The chemical composition of raw clay was characterized by Atomic Absorption Spectrometry (AAS-model, spectra AA-20 plus), the functional/compositions of the samples were determined by Fourier Transform Infrared Spectroscopy (FTIR) (FT/IR-6600 type A), Morphology of the samples were characterized by Scanning Electron Microscopy (SEM) (Shi-madzu COXIEM-30, Japan ), UV-visible DRS (Shi-madzu UV-3600Plus, Japan).

## 3.4. Photocatalytic activities

The photocatalytic activities of the synthesized samples were evaluated as reported by Xu *et al* [59]. The details experimental set up is as follows; 0.025 g of synthesized catalyst was mixed with 125 mL of Methylene Blue solution (10 ppm). Then, the solution was sonicated for 30 minutes under dark till adsorption-absorption equilibrium between photocatalyst and MB is reached before its exposed to irradiation. The incandescent halogen lamp with power sources of 150 W was used as a source of visible light and circulating water to cool the glass reactor. After irradiation is started, 5 mL of the aliquot solution were taken out from the mixture at the uniform irradiations interval and the catalyst was separated from the suspensions by centrifugation. Finally, the degradation was controlled by UV-vis absorbance Spectroscope and measure absorbance of MB. The concentrations of the MB left in the solution was calculated by using the value of maximum absorbance at wavelength ( $\lambda_{max}$ = 663 nm) from the spectra and then, percent of degradation ( D %) equation was used as follows [59] ;

$$D\ \% = \frac{A_o - A_t}{A_o} \times 100\ \%$$

Where D % degradation rate, $A_o$ is the initial absorbance of MB and $A_t$ is the absorbance of MB after time "t" in minutes. For the comparison purpose, all other catalysts were tested in similar manner.

The reusability of the catalyst was also tested. In details, 125 mg of 10CZK catalyst was added to the 625 mL of Methylene Blue (10 ppm) and the mixture was sonicated for 30 min. Subsequently, the resulting mixture was exposed to the visible light for 105 min. Then, 5 ml of aliquot solution was taken out from the mixture after the irradiation time is reached. After the catalyst was settled at the bottom of the beaker, the supernatant was decanted and the catalyst was reused for the next cycle.

# CHAPTER 4
# RESULTS AND DISCUSSION

## 4.1. Thermal analysis

Thermal stability of the kaolin was analysed by DTG. Figure 4.1 (a-b), shows the thermal stability of kaolin sample heated from room temperature to 1000 ℃ at a rate of 10 ℃/min in platinum cup and other empty platinum cup was used as a control. As shown from Figure 4.1 (b), The DTA curve shows the small endothermic peaks around 95 ℃ which may be occurs due to the volatile organic compounds present in it and/or can be due to the hygroscopic water [162]. Also, it can be observed that, small additional endothermic peaks about 261.76 ℃ depict may be the presence of gibbsite sheet. The kaolin to Metakaolinite phase transition characteristics is demonstrated by the intense peaks observed near 500 ℃ [18, 61].

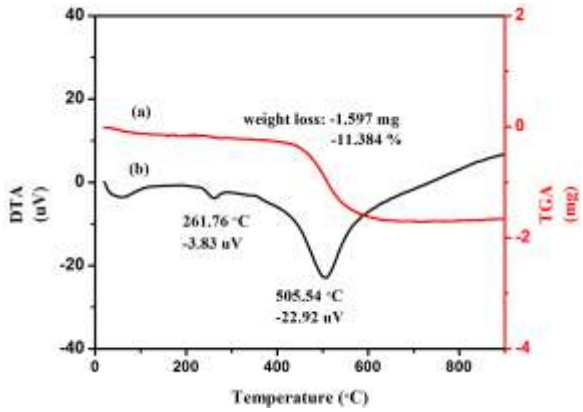


Figure 4.1 Thermal analyze of Bo-Kaolinite; (a).TGA (b) DTA

As we have seen from Figure 4.1 (a), Below 400℃, the indicated weight losses correspond to the hygroscopic water losses from the surface of kaolin or the removal of volatile organic compounds. The major weight losses between 400 – 660 ℃ which is about -11.384 wt % is due to the dehydroxylation of kaolinite during the phase transformation to Metakaolinite [18]. Between these temperatures, the structural changes of the octahedral

Aluminium sheet with dehydroxylation of loss of OH structure of kaolin are expected. This phase transformations of kaolinite to metakaolinite is confirmed by the XRD patterns as shown in Figure 4.2 (a), which is calcined at 600 ℃ for 1hr. 600 ℃ is a temperature at which complete formation of metakaolinite phase is observed. The temperature range of kaolinite to metakaolinite phase transformation is in the range of 420-660 ℃,

$$Al_2O_3.2SiO_2.2H_2O \xrightarrow{420\text{-}660\,℃} Al_2O.2SiO_2 + 2H_2O$$

Kaolinite metakaolinite

## 4.2. Atomic absorption spectrometer (AAS).

The chemical compositions of kaolin raw material were measured by using atomic absorption spectroscopy (AAS). AAS result revealed that kaolinite sources contain high amounts of $Al_2O_3$ and $SiO_2$ contents, 32.16 and 49.86 %, respectively. To identify the types of clay it is important to know the ratio of $SiO_2$ to $Al_2O_3$ as they are major oxides compared to other oxides present. The ideal molar ratio of $SiO_2/Al_2O_3$ for chemically pure kaolinite is 2:1 [40]. However, Table 4.1 revealed that the ratio of $SiO_2/Al_2O_3$ is about 1.5, which may be due to the mixtures of minerals and non-minerals clay present in kaolin clay [40]. Hence, the AAS results prove that the selected clay is kaolinite clay minerals. The LOI observed in Table 4.1 also considerably consistant with TGA result as shown in Figure 4.1 (a). AAS analysis also illustrates that the major and minor oxides ($SiO_2$, $Al_2O_3$, $Fe_2O_3$, CaO, MgO, $Na_2O$, $K_2O$, $TiO_2$, MnO, $P_2O_5$, ) in percentage as shown in Table 4.1.

Table 4.1 Chemical compositions of raw kaolin

| Oxides | $SiO_2$ | $Al_2O_3$ | $Fe_2O_3$ | CaO | MgO | $Na_2O$ | $K_2O$ | MnO | $P_2O_5$ | $TiO_2$ | $H_2O$ | LOI |
|---|---|---|---|---|---|---|---|---|---|---|---|---|
| composition (%) | 49.86 | 32.16 | 0.44 | <0.01 | 0.10 | <0.01 | 0.46 | <0.01 | 0.04 | 0.04 | 2.95 | 12.80 |

Note: Loss of ignition (LOI)

## 4.3. Structure and phase analysis of samples

The XRD patterns of normal kaolin (N), pure kaolinite (P), and calcined kaolinite (H) were also shown in Figure 4.2 (a). Figure 4.2 (a) illustrates the XRD patterns for the normal kaolin clay show the presence of kaolinite type clay minerals with small additions of impurities such as quartz, feldspar and gibbsite sheet (JCPDS: 00-058-2030). The higher intensity associated with kaolinite minerals observed shows the dominance of kaolinite type minerals over other non-minerals kaolin clay such as quartz, feldspar and gibbsite sheet [18, 61]. However, the purified clays illustrate the non-appearance of other non-clay minerals (JCPDS: 00-029-1487) ( Figure 4.2. (a)). This is due to the clay fraction ( particle size 2 $\mu$) that used to separate clay minerals from non clay minerals [162]. After heat treatment the kaolin depicts amorphous structure as observed from the XRD results (Figure 4.2 (a). The major characteristics reflections of kaolinite is observed at about $2\theta$ of $12.20°$, $20.24°$, and $24.70°$, which is associated with (001), (100), and (002), respectively. These major peaks and other peaks correspond to the characteristics of kaolinite is transformed to metakaolinite characteristic peaks, which are narrowed due to the loss of hydroxide structure during the calcination process.

Moreover, the XRD patterns of ZnO, $Cu_2O$, and other composites like ZK, 5CZK, 10CZK, 15CZK and 20CZK are also shown in Figure 4.2 (b). For pure ZnO, the major diffraction peaks are illustrated at $31.76°$, $34.43°$, $36.25°$, $47.54°$, $56.59°$, $62.86°$, $66.37°$, $67.95°$ and $69.08°$, which associated with (100), (002), (101), (102), (110), (103), (200), (112), and (201) planes of hexagonal wurtzite ZnO (JCPDS:00-036-1451), respectively. For pure $Cu_2O$, the major peaks are located at $29.59°$, $36.45°$, $42.33°$, $61.41°$, $73.56°$, and $77.42°$, corresponding to (110), (111), (200), (220), (311), and (222) planes of cubic $Cu_2O$ phase (JCPDS: 00-005-0667), respectively.

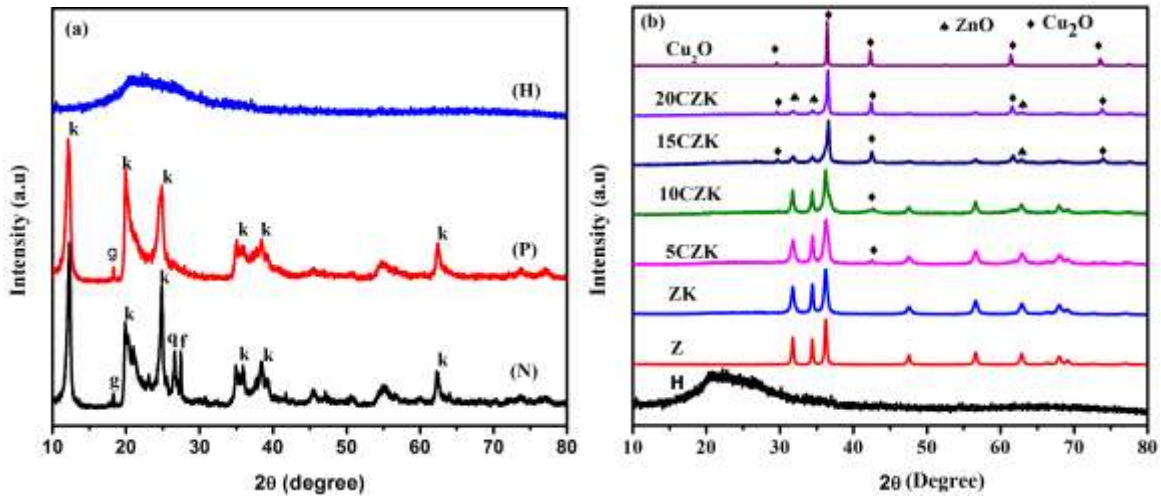


Figure 4.2 XRD pattern for (a), normal kaolin (N), pure kaolinite (P), calcined kaolinite (H). and (b). ZnO, ZnO/kaolinite composite, ZnO/kaolinite with varied of added $Cu_2O$ (termed 5CZK, 10CZK, 15CZK and 20 CZK) composite and $Cu_2O$ (termed C)

Moreover, the ZnO/kaolinite, the crystal structures of ZnO are maintained after calcination but broadening g which may be caused by recrystallization and growth of ZnO. For all ternary composites, (i) ZnO peaks are observed, which decreased with increased contents of $Cu_2O$, (ii) $Cu_2O$ peaks are observed, (iii) disappearing of peaks corresponding kaolinite phase, which match with the result reported by Shvarzman *et al.[163],* Y.-H. Zhang, *et al.[40]* and Fernandez *et al.* [164], due to the dehydroxylation process and following the transformation of kaolinite to metakaolinite phase. These results proved the formation of composite from ZnO, $Cu_2O$, and kaolinite. The aforementioned reasons reveal the growth of ZnO on the kaolinite and subsequently, $Cu_2O$ on the ZnO/kaolinite. The crystallite sizes of all samples were calculated using the Scherrer formula with assumption of uniform crystalline size and shape [40];

$$D = \frac{0.9\lambda}{\beta COS\theta}$$

Where, D crystallite size, $\lambda = 1.54178\,\AA$ is the wavelength of X-Ray (0.1540 nm), β is FWHM (full width at half maximum), θ is diffraction angle. The result is tabulated in Table 4.2.

It can be seen that in Table 4.2, the smaller grain size was observed after the introduction of kaolinite. The reduced grain sizes of ZnO from 28.36 nm to around 18.80 nm was due to the carrier effect of kaolinite. This indicates that the growth of ZnO crystalline is suppressed by natural kaolinite. It is well known that the natural mineral attributes to the retardation of size growth, surface modification and uniform particle dispersion [145]. Among the ternary composites, 5CZK had smaller grain sizes compared to other composite and pure ZnO. The average grain sizes of the as-synthesized catalyst are shown in table 4.2. For the photocatalytic activities not only smaller grain is needed but also the suitable amount of catalyst loaded will leads to the best photocatalytic activity [165].

Table 4.2 The average crystalline sizes of the as-synthesized catalysts

| Code | Z | ZK | 5CZK | 10CZK | 15CZK | 20CZK | C |
|---|---|---|---|---|---|---|---|
| D (nm) | 28.36 | 18.80 | 14.55 | 18.47 | 21.75 | 31.59 | 50.65 |

## 4.4. FTIR and DRS analysis

The composition/functional properties of the samples were characterized by FTIR as shown in Figure 4.3 (a). Regarding the general features of Kaolin, the O-H stretching is strongly connected to the kaolin [166]. As observed from Figure 4.3 (a), the characteristic bands of kaolinite at high wave numbers 3699 and 3626 $cm^{-1}$ may associate with the inner octahedral structure of Al-OH, and stretching mode of O-H that exist in the crystalline of the hydroxyl group, H-O-H stretching adsorbed water is located at about 3444 $cm^{-1}$, 3524 $cm^{-1}$, and 1633 $cm^{-1}$, the peaks assigned at 912 $cm^{-1}$ and 696 $cm^{-1}$ may correspond to O-H deformation linked to $2Al^{3+}$ and Si-O quartz, respectively [160, 166]. Si-O-Al bending vibrations were assigned at 540 $cm^{-1}$ and 755 $cm^{-1}$ [150]. Peaks assigned at 793 $cm^{-1}$, 753 $cm^{-1}$, and 690 $cm^{-1}$ are as a result of O-Al-H vibrations [160]. Si-O network vibration modes are assigned at peaks of 1115, 1032, and 1009 $cm^{-1}$ [150]. As observed in Figure4.3 (a), the broad peak assigned between regions of 3650-3030 $cm^{-1}$ is due to the presence of hydroxyl groups for each spectrum [167] The characteristic peak associated with Zn-O stretching vibration modes is assigned at around 420 $cm^{-1}$ as reported in the literature [160, 168]. The strong Cu-O bonds assigned at 632 $cm^{-1}$[169]. The decreased and shifting of the intensity peaks associate with Si-O vibrations modes at 1032 $cm^{-1}$ implies a good attachment of ZnO

on the kaolinite. Further loading of $Cu_2O$ also shows a similar pattern with further decreasing and shifting to higher wavenumbers which proved of $Cu_2O$ immobolized on ZnO/kaolinite.

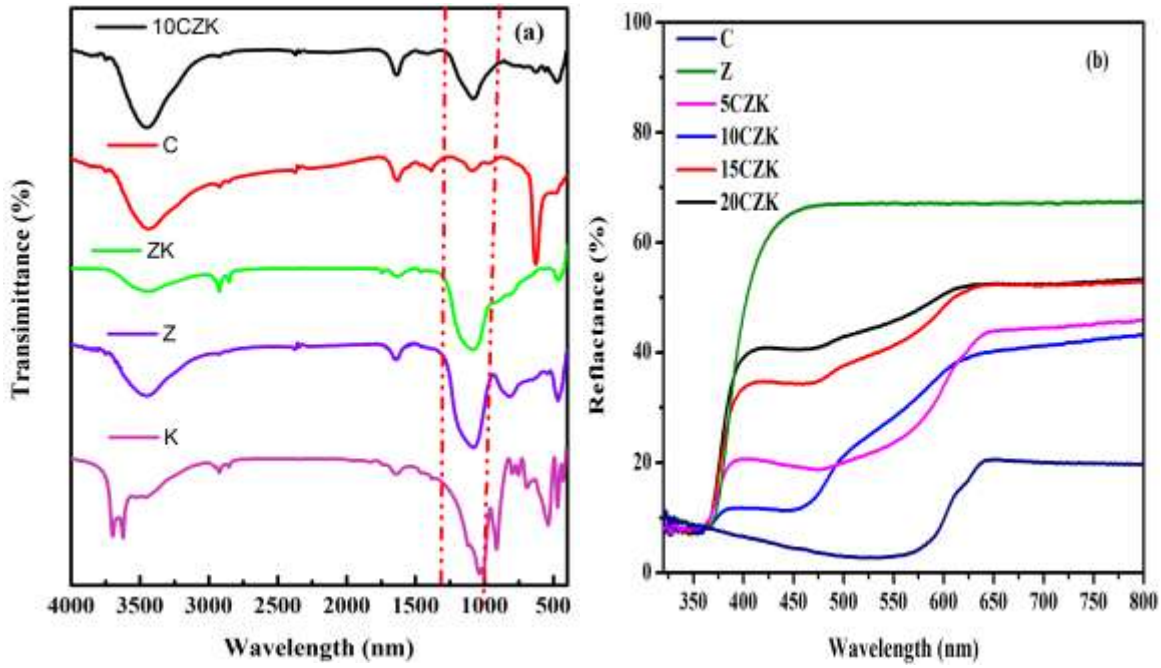


Figure 4.3 (a) FTIR Spectra of K, Z, C, ZK and 10CZK, (b) UV-visible DR Spectra of C, Z, 5CZK, 10CZK, 15CZK and 20CZK

Figure 4.3 (b) shows the absorption spectra of ZnO, $Cu_2O$, and the composite synthesized with various amounts of $Cu_2O$. For pure ZnO, the absorption edge at 380 nm was observed as shown in Figure 4.3 (b). Moreover, the absorption egdes of $Cu_2O$/ZnO/Kaolinite shows redshifted compared to pure ZnO, and broad absorption in visible region as illustrated in Figure 4.3 (b). This effects originated from the introduction of $Cu_2O$ to ZnO. Also, band-gaps of the synthesized samples are calculated by using Kubalk-Munk equation. As shown in Appendix I. the estimated band-gaps for pure $Cu_2O$, and ZnO, are 1.94 eV, 3.22 eV, repectively. The observed narrower bandgaps are mainly attributed to the intimate interfacial contact between $Cu_2O$ and ZnO, which inturn reduce electron-hole recombination and made them visible light driven (Appendix I).

## 4.5. Morphology of the prepared samples

The morphology and microstructures of the synthesized samples were studied by using the scanning electron microscope. The obtained results are shown in Figure 4.4 (a-d). As observed in Figure 4.4 (a), the kaolinite exhibit flat, and smooth surface. Figure 4.4 (b), pure ZnO face down to agglomerate and aggregate due to its small size and high surface energy.

The observed microgarphs looks like smaller rods compacted together. For pure $Cu_2O$, uniform smaller cubic shape attached to each other is shown in Figure 4.4 (c). Figure 4.4 (d), the morphology of ternary composite Moreover, the elemental map analysis of $Cu_2O$/ZnO/kaolinite (10CZK) catalysts are shown by using Energy Dispersive X-ray Spectroscopy (EDS) in Figure 4.4, (e). the obtained resuts much with the XRD results and the formation of composites can be confirmed.

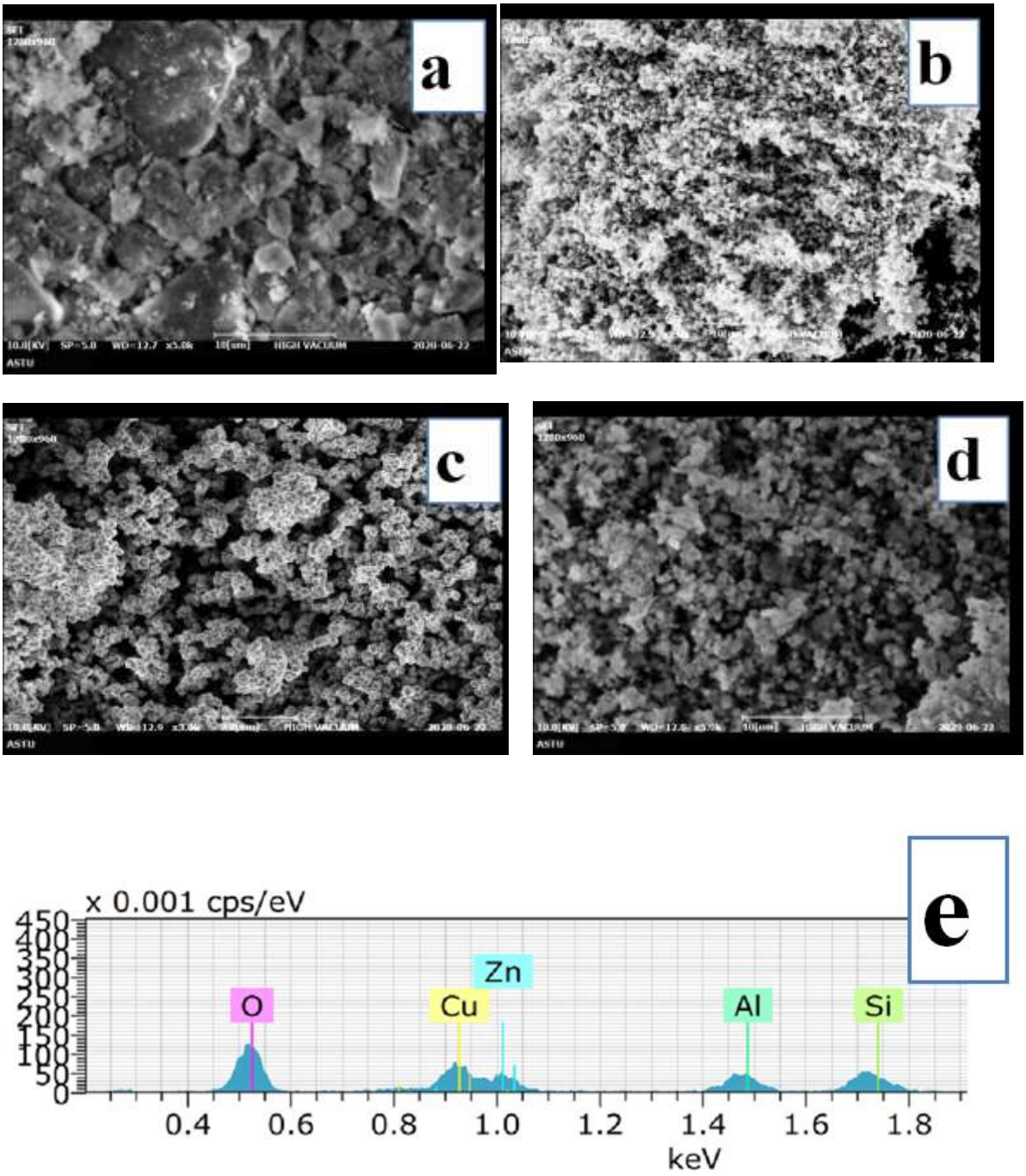


Figure 4.4 SEM image of: (a) K, (b) pure Z, (c) pure C, and (d) 10CZK as-synthesized samples (e) EDS of 10CZK

## 4.6. Photocatalytic activities

To evaluate the photocatalytic activities of the as-synthesized samples, Methylene Blue was selected as a model organic pollutant under Visible light. In the absence of catalysts (blank), the shift in MB concentration did not occur under visible light. However, the degradation of dye was observed in the presence of the photocatalysts. The photocatalytic activities of different catalysts are shown in Figure 4.5 under Visible light. Figure 4.5 (a-d) shows the change in the concentration of MB dye at different intervals of time in the presence of K, Z, C, and 10CZK catalyst respectively. Moreover, for some catalysts shown in Appendix II. Kaolinite exhibited high adsorption during adsorption-desorption and no change in concentration was observed after illumination of light shown in Figure 4.5 (a). For pure ZnO the observed change in concentration is very low as it is inactive under visible light. However, $Cu_2O$ and 10CZK show the change in concentrations of pollutants under visible light as observed in Figure 4.5 (c-d).

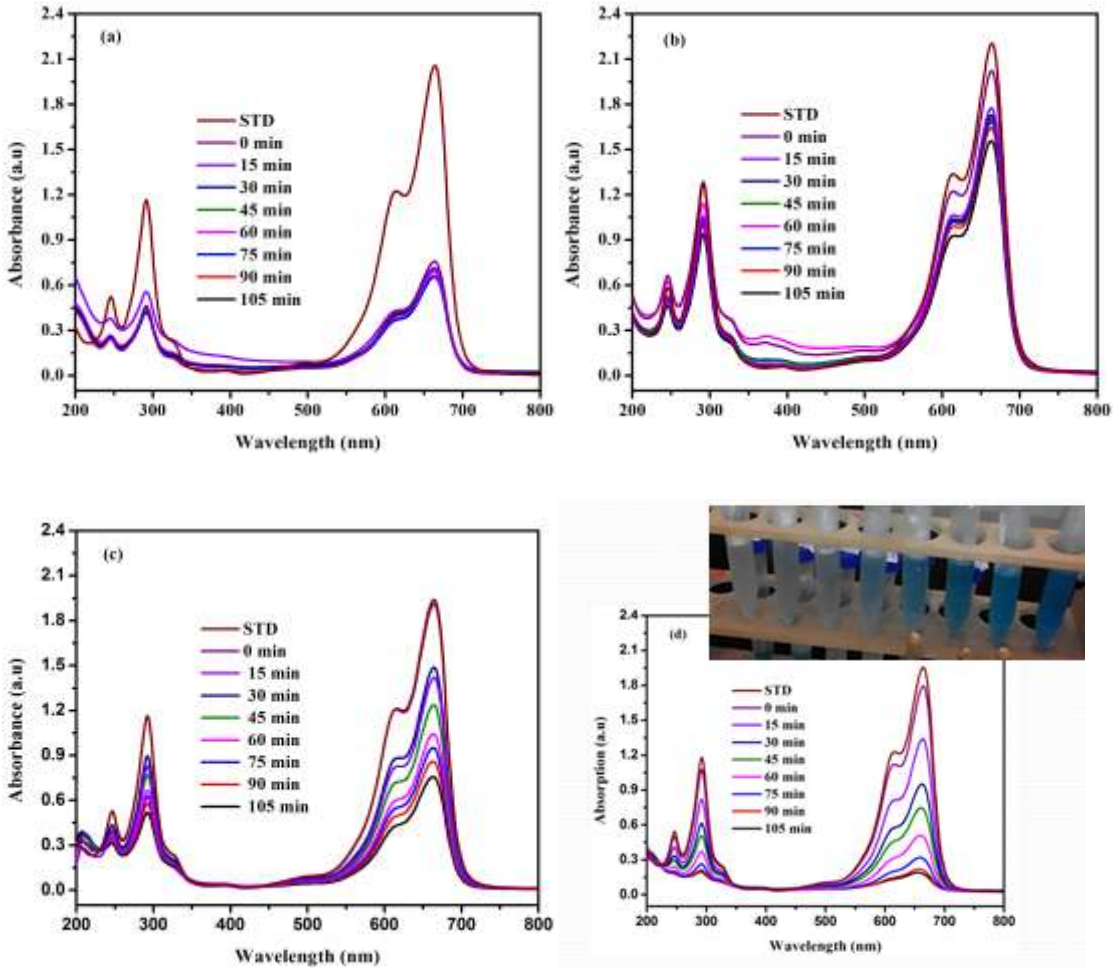


Figure 4.5 UV-Visible absorption spectra for (a) K, (b) Z, (c) C, (d) 10CZK catalyst after different time irradiations.

Moreover, the $C_t/C_o$ (where Co is initial concentrations after adsorption-desorption equilibrium and $C_t$ is the dye concentration after the irradiated time (in a minute), and the first order-kinetics for different catalyst samples with the degradation of MB and the k value for each catalyst in per-minute is illustrated in Figure 4.6 (a), (b) and (c).

As it is illustrated in Figure 4.6 (a), the degradations of methylene blue dye without a catalyst is negligible and no concentration change is observed at different irradiations time for 105 minutes. Also, for pure kaolinite, the removal is around 62% under dark conditions due to its high adsorption capacity. However, no photocatalytic activity of pure kaolinite is observed after light illumination and this shows that kaolinite is a good adsorbent for methylene blue which reveals good agreement with result reported by Wongso *et al.* [170]. For this reason, kaolinite was selected as a good adsorbent throughout photodegradation and the catalyst (ZnO, $Cu_2O$) for photocatalytic activities. The photocatalytic activity of ZnO is low under visible light due to its wide bandgap. Hence, a low percent of degradation around 28 % is observed for ZnO among the synthesized catalyst. However, with the additions of kaolinite as adsorbent, photodegradation percent of ZK is reached around 50% due to the high adsorption of kaolinite. Besides, in the presence of CZ, 5CZK, 10CZK, 15CZK and 20CZK composite catalysts, 66 %, 76 %, 93 %, 71 %, and 68 % were degraded, respectively.

As we have seen from $C_t/C_o$ graph Figure 4.6 (b), at the beginning the additions of $Cu_2O$ will enhance the photocatalytic activities towards the degradation of methylene blue dye. However, further increasing of $Cu_2O$ leads to the relatively low percent of degradation among the ternary composite. Hence, the optimum amount or maximum limit of $Cu_2O$ loaded on ZnO/Kaolinite (ZK) composite is about 10% for the preparation of 10CZK composite. Besides, the photocatalytic activities of individual *n*-type and *p*-type loaded on kaolinite are relatively weak. Also, the degradation activity of $Cu_2O$ was not significant. However, the formation of *p-n* heterojunctions and the high adsorption capacity of kaolinite were much more efficient than others. The formation of *p-n* heterojunction by a combination of $Cu_2O$ and ZnO can lower the electron-hole recombination which in turn increases the photocatalytic activities [171]. For photocatalytic activity, the synergetic effects of adsorption capacity and photodegradation are the main key points. Therefore, the highest performance observed for 10CZK is due to the synergetic effects and the formation of heterojunctions between $Cu_2O$ p-type and ZnO n-type. Moreover, kaolin can adsorb within its interlaminar layer and on its external surfaces, kaolin can act as electron trapping due to the presence of $Al^{+3}$ in which act as lewis acid, and the presence of active species like Si-O and $^{-}OH$).

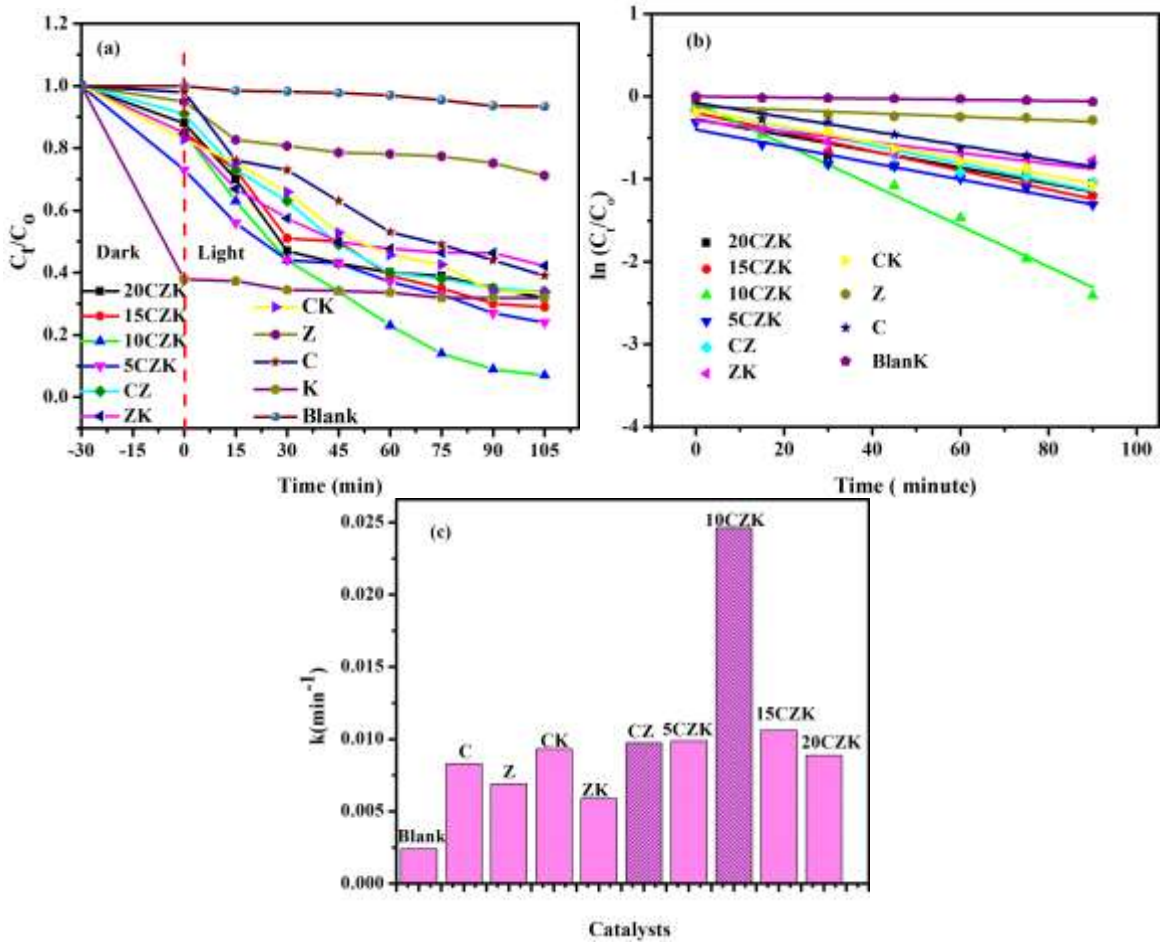


Figure 4.6 (a) The $C_t/C_o$ photodegradation results of MB (10 ppm), (b) Pseudo first-order reaction kinetics rates of MB, (c) the k value in $min^{-1}$ for all synthesized samples

Additionally, Figure 4.6 (b-c) shows the kinetics curve data degradation of methylene blue dye fitting with pseudo-first-order reaction calculated as $-\ln(C_t/C_o) = kt$ (where $C_o$ is initial concentration after adsorption-desorption equilibrium and $C_t$ is the dye concentration after the irradiated time (in a minute), and k the rate constant. The linear relationship between irradiation times and $\ln(C_t/C_o)$ shows that the photocatalytic reaction follows the pseudo-first-order kinetics [172]. The estimated rate constant value for the degradations of MB dyes with Blank (no catalyst), C, Z, CK, ZK, CZ, 5CZK, 10CZK, 15CZK, and 20CZK were 0.00241, 0.00829, 0.00691, 0.00931, 0.00588, 0.00975, 0.00988, 0.02463, 0.0106, and 0.00887 $min^{-1}$ respectively as shown in Figure 4.6 (c). As observed from this data the rate constant of 10ZCK is 25.3 times higher than ZC without kaolinite. This reveals that the photocatalytic degradations of MB by 10CZK is much higher than that of CZ without kaolinite under visible light.

## 4.7. Stability and reusability of the catalyst

Having noticed that the synthesized composite reveals the enhanced photocatalytic activities, evaluating its stability and reusability are the main two points. Moreover, in terms of economic and environmental points of view, it is important to test the stability and reusability of any catalyst. To analyze these properties, 10CZK composite catalyst was selected for the degradations of methylene blue. In details, 125 mg of the catalyst with 625 mL of methylene blue solution (10 ppm) was used. The catalyst was separated by washing using centrifuge, dried and reused for the next cycle repeatedly after every experimental run. As shown in Figure 4.7, no significant decrement was observed for the photocatalytic degradation efficiency of 10CZK for methylene blue even after 5$^{th}$ round. The degradation efficiency observed for 1$^{st}$, 2$^{nd}$, 3$^{rd}$, 4$^{th}$, and 5$^{th}$ rounds were 93, 88, 87, 85, and 83 %, respectively. This efficient stability is due to the presence of kaolin, strong attachment of $Cu_2O$/ZnO on the kaolinite matrix. Hence, the synthesized 10CZK catalyst reveals the enhanced photocatalytic activities including reusability.

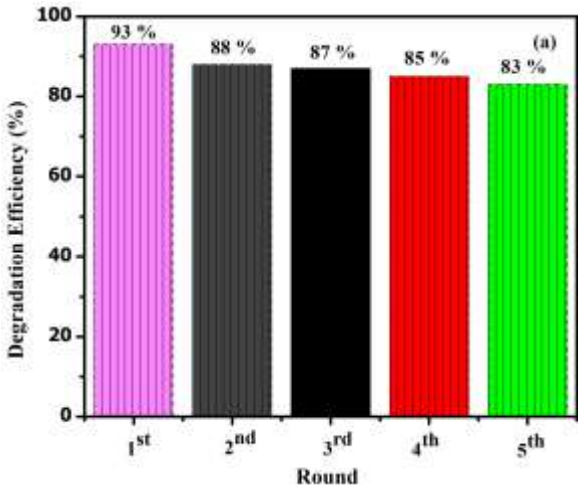


Figure 4.7 Photocatalytic reusability and stability of 10CZK for the degradations of methylene blue dye (10 ppm)

The active species such as superoxide anion radicals ($O_2^-$), holes ($h^+$), electrons ($e^-$) and hydroxyl radicals ($^{\cdot}OH$) are very important in the photodegradation of organic pollutants and play a fundamental role in the photocatalytic reaction [173, 174]. Accordingly, to identify the role of active radicals during the photocatalytic degradation the trapping experiment for active species was carried out by using 10CZK composite. These selected trapping agents were $AgNO_3$, EDTA and IPA for scavenging electron ($e^-$), holes ($h^+$) and OH radicals respectively [173, 174]. As observed from the trapping experiment, Figure 4.8 (a), the additions of IPA had an insignificant effect on the photocatalytic degradation efficiency compared to the catalyst without scavengers. Therefore, OH radicals can not act as major active species even if produced among crucial reactive species during the photodegradation process. However, the additions of both EDTA and $AgNO_3$ lowers the photocatalytic activities. This reveals that the major active species for the degradation of MB are both $h^+$ and $e^-$ compared to hydroxyl radicals added to the 10CZK catalyst.

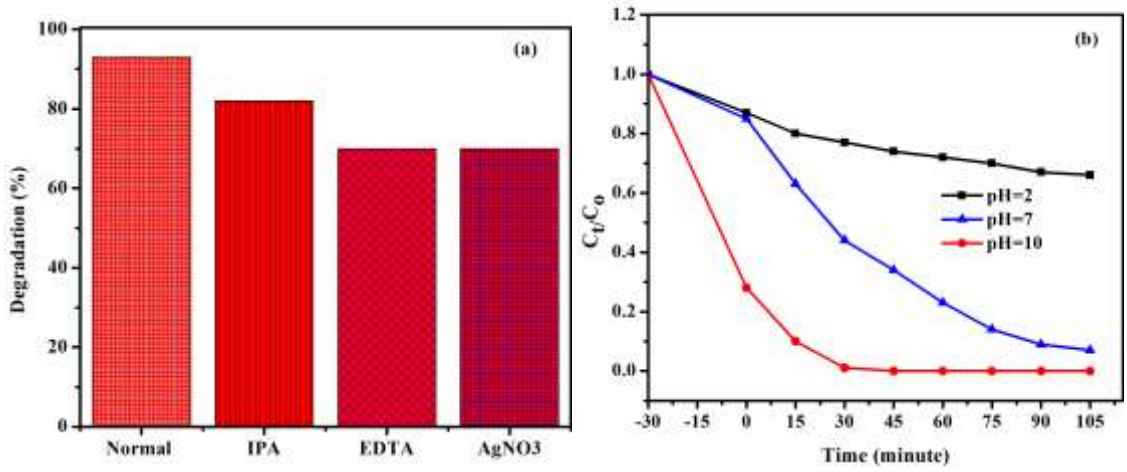


Figure 4.8. (a) Reactive oxygen species (ROS) scavenging experiments with 10CZK catalyst under visible light, (b) the $C_t/C_o$ plot with irradiations of time in acidic, neutral and basic media.

Moreover, the effect of pH on the photocatalytic degradations of 10CZK was studied in acidic, neutral, and basic media. The pH value is adjusted by the additions of NaOH or HCl. As shown in Figure 4.8 (b), the catalyst shows complete degradation in basic media (pH=10) within 30 min, in neutral condition 93 % and acidic media lower degradation efficiency and had insignificant compared to others media. This is due to the minimum adsorption of Methylene blue in acidic media. The highest adsorption of MB dye observed for in basic media is may be due to the favourable conditions of cationic dyes in basic sites [175]. The

surface of kaolinite is modified with the increasing of pH from acidic to basic media, which allows as the clay uptake more MB dye. Also, the electrostatic attraction between the negative surface of kaolinite and dissociate cationic dyes leads to almost 100 % of MB adsorption and can be completely degraded [175].

## 4.8. Possible mechanisms of photodegradation

Based on the aforementioned reason, the possible photodegradation efficiency of MB by $Cu_2O$/ZnO/kaolinite is shown in Figure 4.9. For pure ZnO and $Cu_2O$, the electrons-holes generated will tend to recombine and then reduce the photocatalytic activities [171, 176]. However, for the synthesized ternary composite 10CZK, the structure was well established and the chemically bonded interfacial contacts between the catalyst and kaolinite were achieved for the composites. The ability to harvest the solar spectrum and the adequacy of the electron-hole pairs generated for reactive oxygen species are the two main crucial for the photocatalytic activities [177]. Herein, for the improvement of photocatalytic activities both light-harvesting and enhancement of the electron-hole separations were considered as the main factor. $Cu_2O$ is a *p*-type owing to its lower bandgap energy has strong adsorption in visible light [178]. Hence, combined *n*-type ZnO with *p*-type $Cu_2O$ can possess great potentials for the photodegradation activities under visible light. The formation of p-n heterojunctions can reduce the electron-hole recombination during excitation under visible light. Moreover, negatively charged surface of kaolinite would be important for the electron-hole separation due to the electrostatic repulsion [49].

Also, due to the presence of Al atoms in the kaolinite structure, the photogenerated electrons can be trapped by Al atoms. That means kaolin can used as electron acceptor because of lewis acids present (Al atoms) [179, 180]. On the other hand, due to the presence of excess hydroxyl ions on the surface kaolinite the new bond would be formed as Zn-O-H during the preparation of composite which may be beneficiary for the separation of carriers [161]. Therefore, the generated electrons in the Conduction band of $Cu_2O$ could reduce the adsorbed oxygen and produce more oxygen radicals. Also, the adsorbed oxygen could react with electrons and water molecules to generate hydrogen peroxide ($H_2O_2$). Some of these generated oxygen radicals ($O_2^{\bullet -}$) and hydrogen peroxide ($H_2O_2$) further changed to the active species called hydroxyl radicals ($^{\bullet}OH$). Moreover, the holes ($h^+$) left on the valence band of ZnO could react with water molecules to generate hydroxyl radical active species. In our case, both electrons and holes are the major active species, and oxygen radical is subordinate

active species. These main and subordinate active species could enhance the photocatalytic activities of the ternary composite for the effective and efficient degradations methylene blue dye under visible light.

The governed equations are summarized as shown in equation (1-7):

$$Cu_2O/ZnO + hv = Cu_2O\ (h_{VB}^{+}) + ZnO\ (e_{CB}^{-}) \quad (1)$$

$$ZnO\ (e_{CB}^{-}) + O_2 = ZnO + O_2^{\cdot -} \quad (2)$$

$$Cu_2O\ (h_{VB}^{+}) + OH^{-} = {}^{\cdot}OH + Cu_2O \quad (3)$$

$$O_2^{\cdot -} + H_2O = HO_2^{-} + {}^{\cdot}OH \quad (4)$$

$$HO^{-} + H_2O = H_2O_2 + {}^{\cdot}OH \quad (5)$$

$$H_2O_2 = 2\,{}^{\cdot}OH \quad (6)$$

$$Dye\ (MB) + {}^{\cdot}OH = CO_2 + H_2O \quad (7)$$

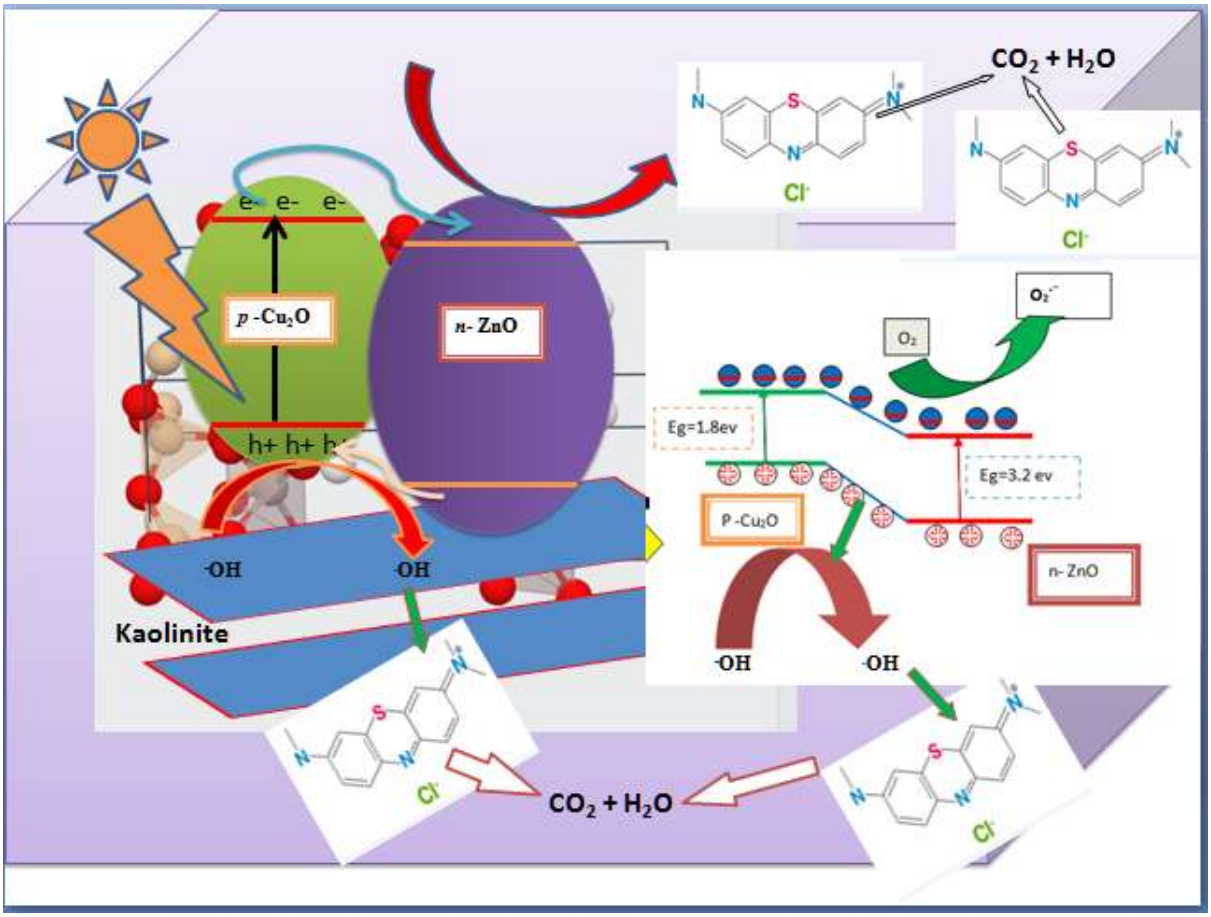


Figure 4.9 Schematic representation of a possible mechanism for the enhancement of photodegradation of Methylene blue dye by Cu2O/ZnO/Kaolinite composite under visible light.

# CHAPTER 5

# CONCLUSION AND RECOMMENDATIONS

## 5.1. Conclusion

A novel $Cu_2O$/ZnO/kaolinite composite was successfully synthesized by a simple and cost-effective method called Co-precipitation method. The formation of the composite was confirmed by SEM, XRD, and FTIR characterization techniques. On the other hand, the chemical compositions of kaolin clay were characterized by AAS and confirmed the selected clay is Kaolin. Also, UV-visible spectroscopy was used to measure the concentrations of pollutants decreased concerning irradiation times. The absorbance of composite in the visible region was also evaluated by UV-visible DR Spectroscopy.

The absorption egdes of $Cu_2O$/ZnO/Kaolinite composite shows redshifted compared to pure ZnO, and broad absorption in visible region. The as-synthesized $Cu_2O$/ZnO/Kaolinite (10CZK) composite exhibited enhanced photocatalytic activity towards the degradations of Methylene blue under visible light illumination. The enhancement photocatalytic activity should be attributed to (1) improvement of light-harvesting, (2) electron-hole separations, (3) synergetic effects of Composite (adsorption-degradation activity). Hence, in our study, the optimum ternary catalyst was achieved by loading 10 % of Cu2O on the ZnO/kaolinite composite with appropriate conditions. The composite exhibited high photocatalytic activities in basic media (pH=10 ). The good reusability of composite after $5^{th}$ cycle indicates that the recyclability and stability of the synthesized ternary composite.

Furthermore, Scavengers experiment demonstrates the reactive species for the degradation purposes are electrons and holes rather than hydroxyl radicals. Based on the scavangers experiment the possible mechanism for the degradation process of methylene blue was designed. This study provides improved efficient-visible light driven ternary composite, which exhibit high photocatalytic activities towards the degradations of organic pollutants and proves the practical applications of the synthesized composite for industrial applications.

## 5.2. Recommendation

The following things are the main challenges that should be considered :

- ✓ Further morphology of the catalyst should be analyzed with high magnification microscope.
- ✓ Photoluminenscence (PL) spectrometry should be needed to confirm further the separation of electron-hole pairs.
- ✓ Confirmation of *p*-*n* junction formation is also needs further characterization.
- ✓ TEM and XPS analysis should be carried out for further information.
- ✓ BET analysis is also important to determine surface area of the synthesized catalyst.
- ✓ For real application its possible to evaluate under solar light as we have enough resources of clay.

# REFERENCE


[1] C. Becerra-Castro, A.R. Lopes, I. Vaz-Moreira, E.F. Silva, C.M. Manaia, O.C. Nunes, Environment international 75 (2015) 117-135.

[2] Q. Wang, Z. Yang, Environmental pollution 218 (2016) 358-365.

[3] E.S.Z. El-Ashtoukhy, N.K. Amin, M.M. Abd El-Latif, D.G. Bassyouni, H.A. Hamad, Journal of Cleaner Production 167 (2017) 432-446.

[4] A.d.l. Fuente, A.M. Muro-Pastor, F. Merchán, F. Madrid, J.I. Pérez-Martínez, T. Undabeytia, Journal of Cleaner Production (2019) 117964.

[5] D. Lv, L. Zheng, H. Zhang, Y. Deng, Environmental Science: Water Research & Technology 4 (2018) 701-710.

[6] J. Ma, R. Wang, X. Wang, H. Zhang, B. Zhu, L. Lian, D. Lou, Journal of Environmental Chemical Engineering 7 (2019) 103049.

[7] T. Lou, X. Yan, X. Wang, International Journal of Biological Macromolecules 135 (2019) 919-925.

[8] T. Nie, P. Hao, Z. Zhao, W. Zhou, L. Zhu, Science of The Total Environment 673 (2019) 522-532.

[9] M. Wiśniewski, A. Bieniek, P. Bolibok, S. Koter, P. Bryk, P. Kowalczyk, A.P. Terzyk, Microporous and Mesoporous Materials (2019) 109649.

[10] S. Chaudhury, V.G. Mishra, D.J. Shah, Journal of Water Process Engineering 31 (2019) 100896.

[11] W. Raza, J. Lee, N. Raza, Y. Luo, K.-H. Kim, J. Yang, Journal of Industrial and Engineering Chemistry 71 (2019) 1-18.

[12] X. Li, M. Cai, L. Wang, F. Niu, D. Yang, G. Zhang, Science of The Total Environment 659 (2019) 1415-1427.

[13] L.A. Betancourt-Buitrago, O.E. Ossa-Echeverry, J.C. Rodriguez-Vallejo, J.M. Barraza, N. Marriaga, F. Machuca-Martínez, Photochemical & Photobiological Sciences 18 (2019) 853-862.

[14] S. Talwar, V.K. Sangal, A. Verma, Journal of Photochemistry and Photobiology A: Chemistry 353 (2018) 263-270.

[15] Z. Cheng, S. Zhao, L. Han, Nanoscale 10 (2018) 6892-6899.

[16] S. Dong, J. Feng, M. Fan, Y. Pi, L. Hu, X. Han, M. Liu, J. Sun, J. Sun, RSC Advances 5 (2015) 14610-14630.

[17] G. Ye, Z. Yu, Y. Li, L. Li, L. Song, L. Gu, X. Cao, Water Research 157 (2019) 134-144.

[18] L. Ayele, J. Pérez-Pariente, Y. Chebude, I. Díaz, Applied Clay Science 132-133 (2016) 485-490.

[19] K.M. Lee, C.W. Lai, K.S. Ngai, J.C. Juan, Water Research 88 (2016) 428-448.

[20] X. Chen, H. Sun, J. Zhang, O. Ahmed Zelekew, D. Lu, D.-H. Kuo, J. Lin, Applied Catalysis B: Environmental 252 (2019) 152-163.
[21] H. Wang, X. Qiu, W. Liu, D. Yang, Applied Surface Science 426 (2017) 206-216.
[22] R. Mohammadi-Aloucheh, A. Habibi-Yangjeh, A. Bayrami, S. Latifi-Navid, A. Asadi, Journal of Materials Science: Materials in Electronics 29 (2018) 13596-13605.
[23] M.A. Hernández-Carrillo, R. Torres-Ricárdez, M.F. García-Mendoza, E. Ramírez-Morales, L. Rojas-Blanco, L.L. Díaz-Flores, G.E. Sepúlveda-Palacios, F. Paraguay-Delgado, G. Pérez-Hernández, Catalysis Today (2018).
[24] A.K. Chandiran, M. Abdi-Jalebi, M.K. Nazeeruddin, M. Grätzel, ACS nano 8 (2014) 2261-2268.
[25] J.A. Anta, E. Guillen, R. Tena-Zaera, The Journal of Physical Chemistry C 116 (2012) 11413-11425.
[26] C. Hariharan, Applied Catalysis A: General 304 (2006) 55-61.
[27] G. Colón, M. Hidalgo, J. Navío, E.P. Melián, O.G. Díaz, J.D. Rodríguez, Applied Catalysis B: Environmental 83 (2008) 30-38.
[28] C. Lizama, J. Freer, J. Baeza, H.D. Mansilla, Catalysis Today 76 (2002) 235-246.
[29] D. Mijin, M. Savić, P. Snežana, A. Smiljanić, O. Glavaški, M. Jovanović, S. Petrović, Desalination 249 (2009) 286-292.
[30] A. Akyol, H. Yatmaz, M. Bayramoglu, Applied Catalysis B: Environmental 54 (2004) 19-24.
[31] R. Qiu, D. Zhang, Y. Mo, L. Song, E. Brewer, X. Huang, Y. Xiong, Journal of hazardous materials 156 (2008) 80-85.
[32] H. Qin, W. Li, Y. Xia, T. He, ACS applied materials & interfaces 3 (2011) 3152-3156.
[33] A.B. Patil, K.R. Patil, S.K. Pardeshi, Journal of Hazardous Materials 183 (2010) 315-323.
[34] G.R. Andrade, C.C. Nascimento, Z.M. Lima, E. Teixeira-Neto, L.P. Costa, I.F. Gimenez, Applied Surface Science 399 (2017) 573-582.
[35] A. Yarahmadi, S. Sharifnia, Dyes and Pigments 107 (2014) 140-145.
[36] B. Krishnakumar, B. Subash, M. Swaminathan, Separation and Purification Technology 85 (2012) 35-44.
[37] F. Kiantazh, A. Habibi-Yangjeh, Materials Science in Semiconductor Processing 39 (2015) 671-679.
[38] S. Rao, G.S. Shekhawat, Journal of Environmental Chemical Engineering 2 (2014) 105-114.
[39] B.C. Heng, X. Zhao, S. Xiong, K.W. Ng, F.Y. Boey, J.S. Loo, Food Chem Toxicol 48 (2010) 1762-1766.
[40] K. Mamulová Kutláková, J. Tokarský, P. Peikertová, Applied Catalysis B: Environmental 162 (2015) 392-400.
[41] S. Miao, Z. Liu, B. Han, J. Zhang, X. Yu, J. Du, Z. Sun, Journal of Materials Chemistry 16 (2006) 579-584.

[42] Z. Li, W.-T. Jiang, C.-J. Chen, H. Hong, Langmuir 26 (2010) 8289-8294.
[43] Y. Zhang, H. Gan, G. Zhang, Chemical Engineering Journal 172 (2011) 936-943.
[44] D. Bougeard, K.S. Smirnov, E. Geidel, The Journal of Physical Chemistry B 104 (2000) 9210-9217.
[45] R.L. Frost, J. Kristof, J.T. Kloprogge, E. Horvath, Langmuir 16 (2000) 5402-5408.
[46] A. Mishra, A. Mehta, S. Basu, Journal of Environmental Chemical Engineering 6 (2018) 6088-6107.
[47] E. Manova, P. Aranda, M.A. Martín-Luengo, S. Letaïef, E. Ruiz-Hitzky, Microporous and Mesoporous Materials 131 (2010) 252-260.
[48] D. Kibanova, J. Cervini-Silva, H. Destaillats, Environmental science & technology 43 (2009) 1500-1506.
[49] Z. Sun, G. Yao, X. Zhang, S. Zheng, R.L. Frost, Applied Clay Science 129 (2016) 7-14.
[50] J. Niu, A. Wu, D. Wang, L. Zhou, S. Zhang, Z. Liu, P. Feng, X. Ou, Y. Qiang, Materials Letters 230 (2018) 32-35.
[51] X. Dong, Z. Sun, X. Zhang, C. Li, S. Zheng, Journal of the Taiwan Institute of Chemical Engineers 84 (2018) 203-211.
[52] A.J. Misra, S. Das, A.P. Habeeb Rahman, B. Das, R. Jayabalan, S.K. Behera, M. Suar, A.J. Tamhankar, A. Mishra, C.S. Lundborg, S.K. Tripathy, Journal of Colloid and Interface Science 530 (2018) 610-623.
[53] Y. Zhang, B. Deng, T. Zhang, D. Gao, A.-W. Xu, The Journal of Physical Chemistry C 114 (2010) 5073-5079.
[54] A.E. Rakhshani, Solid-State Electronics 29 (1986) 7-17.
[55] Y.-H. Chang, M.-Y. Chiang, J.-H. Chang, H.-N. Lin, Materials Letters 138 (2015) 85-88.
[56] Z. Wang, X. Liang, Y. Zhu, X. Zouhu, X. Feng, R. Zhu, Ceramics International 45 (2019) 23310-23319.
[57] Z. Zheng, B. Huang, Z. Wang, M. Guo, X. Qin, X. Zhang, P. Wang, Y. Dai, The Journal of Physical Chemistry C 113 (2009) 14448-14453.
[58] D. Hong, G. Cao, J. Qu, Y. Deng, J. Tang, Journal of Materials Science & Technology 34 (2018) 2359-2367.
[59] C. Xu, L. Cao, G. Su, W. Liu, H. Liu, Y. Yu, X. Qu, Journal of Hazardous Materials 176 (2010) 807-813.
[60] L. Ayele, J. Pérez-Pariente, Y. Chebude, I. Díaz, Microporous and Mesoporous Materials 215 (2015) 29-36.
[61] A. Merga, H.C.A. Murthy, E. Amare, K. Ahmed, E. Bekele, Heliyon 5 (2019) e02327.
[62] D. Dadi, T. Stellmacher, F. Senbeta, S. Van Passel, H. Azadi, Environ Monit Assess 189 (2017) 11.
[63] M.K. Hasan, A. Shahriar, K.U. Jim, Heliyon 5 (2019) e02145.

[64] S. Shaker-Agjekandy, A. Habibi-Yangjeh, Materials Science in Semiconductor Processing 44 (2016) 48-56.

[65] M. Anjum, R. Kumar, M.A. Barakat, Journal of environmental management 212 (2018) 65-76.

[66] Y. Hai, X. Li, H. Wu, S. Zhao, W. Deligeer, S. Asuha, Applied Clay Science 114 (2015) 558-567.

[67] H. Salari, Journal of Environmental Chemical Engineering 7 (2019) 103092.

[68] K. Wang, H. Li, X. Chen, D. Wan, D. Yan, Y. Ao, Materials Letters 220 (2018) 54-57.

[69] P. Tun, K. Wang, H. Naing, J. Wang, G. Zhang, Applied Clay Science 175 (2019) 76-85.

[70] A. Kumar, P. Lingfa, Materials Today: Proceedings 22 (2020) 737-742.

[71] H. Wang, X. Qiu, R. Zhong, F. Fu, Y. Qian, D. Yang, Materials Chemistry and Physics 199 (2017) 193-202.

[72] H. Irie, T. Shibanuma, K. Kamiya, S. Miura, T. Yokoyama, K. Hashimoto, Applied Catalysis B: Environmental 96 (2010) 142-147.

[73] M.M. Khan, S.F. Adil, A. Al-Mayouf, Journal of Saudi Chemical Society 19 (2015) 462-464.

[74] Aracely Hernández-Ramírez, Iliana Medina-Ramírez.

[75] A. Ibhadon, P. Fitzpatrick, Catalysts 3 (2013) 189-218.

[76] E.M. Samsudin, N.G. Sze, Y.W. Ta, T.L. Tan, S.B. Abd. Hamid, C.J. Joon, Sains Malaysiana 44 (2015) 1011-1019.

[77] O.M. Ishchenko, V. Rogé, G. Lamblin, D. Lenoble, Semiconductor Photocatalysis - Materials, Mechanisms and Applications, 2016.

[78] A. Fujishima, K. Honda, Nature 238 (1972) 37-38.

[79] R. Qian, H. Zong, J. Schneider, G. Zhou, T. Zhao, Y. Li, J. Yang, D.W. Bahnemann, J.H. Pan, Catalysis Today 335 (2019) 78-90.

[80] T. Kamegawa, Y. Ishiguro, H. Seto, H. Yamashita, Journal of Materials Chemistry A 3 (2015) 2323-2330.

[81] L. Wu, Y. Qiu, M. Xi, X. Li, C. Cen, New Journal of Chemistry 39 (2015) 4766-4773.

[82] M. Ye, D. Zheng, M. Wang, C. Chen, W. Liao, C. Lin, Z. Lin, ACS Appl Mater Interfaces 6 (2014) 2893-2901.

[83] Z.L. Wang, Materials today 7 (2004) 26-33.

[84] N. Daneshvar, D. Salari, A. Khataee, Journal of photochemistry and photobiology A: chemistry 162 (2004) 317-322.

[85] V. Kandavelu, H. Kastien, K.R. Thampi, Applied Catalysis B: Environmental 48 (2004) 101-111.

[86] X. Chen, Y. Dai, X. Wang, Journal of Alloys and Compounds 649 (2015) 910-932.

[87] N.N. Yunus, F. Hamzah, M.S. So'aib, J. Krishnan, IOP Conference Series: Materials Science and Engineering 206 (2017).

[88] K.M. Reza, A.S.W. Kurny, F. Gulshan, Applied Water Science 7 (2015) 1569-1578.
[89] S.G. Babu, P. Karthik, M.C. John, S.K. Lakhera, M. Ashokkumar, J. Khim, B. Neppolian, Ultrasonics Sonochemistry 50 (2019) 218-223.
[90] S. Chakrabarti, B.K. Dutta, Journal of Hazardous Materials 112 (2004) 269-278.
[91] V. Rogé, N. Bahlawane, G. Lamblin, I. Fechete, F. Garin, A. Dinia, D. Lenoble, Journal of Materials Chemistry A 3 (2015) 11453-11461.
[92] N. Justh, L.P. Bakos, K. Hernádi, G. Kiss, B. Réti, Z. Erdélyi, B. Parditka, I.M. Szilágyi, Scientific reports 7 (2017).
[93] T. Bora, P. Sathe, K. Laxman, S. Dobretsov, J. Dutta, Catalysis Today 284 (2017) 11-18.
[94] S.T. Tan, A.A. Umar, A. Balouch, M. Yahaya, C.C. Yap, M.M. Salleh, M. Oyama, Ultrasonics Sonochemistry 21 (2014) 754-760.
[95] H. Liu, J. Yang, J. Liang, Y. Huang, C. Tang, Journal of the American Ceramic Society 91 (2008) 1287-1291.
[96] A. Yar, B. Haspulat, T. Üstün, V. Eskizeybek, A. Avcı, H. Kamış, S. Achour, RSC Advances 7 (2017) 29806-29814.
[97] A.P. Shah, S. Jain, V.J. Mokale, N.G. Shimpi, Journal of Industrial and Engineering Chemistry 77 (2019) 154-163.
[98] N.S. Allen, N. Mahdjoub, V. Vishnyakov, P.J. Kelly, R.J. Kriek, Polymer Degradation and Stability 150 (2018) 31-36.
[99] Q. Zhang, L. Gao, J. Guo, Applied Catalysis B: Environmental 26 (2000) 207-215.
[100] L. Gnanasekaran, R. Hemamalini, K. Ravichandran, Journal of Saudi Chemical Society 19 (2015) 589-594.
[101] M.M. Khan, S.A. Ansari, D. Pradhan, M.O. Ansari, D.H. Han, J. Lee, M.H. Cho, J. Mater. Chem. A 2 (2014) 637-644.
[102] N. Kottam, B. Rose Vergis, B.M. Nagabhushana, Materials Today: Proceedings 5 (2018) 20849-20857.
[103] J. Ahmad, K. Majid, New Journal of Chemistry 42 (2018) 3246-3259.
[104] C.H. Nguyen, C.-C. Fu, R.-S. Juang, Journal of Cleaner Production 202 (2018) 413-427.
[105] B. Neppolian, H. Choi, S. Sakthivel, B. Arabindoo, V. Murugesan, Chemosphere 46 (2002) 1173-1181.
[106] L. He, Z. Tong, Z. Wang, M. Chen, N. Huang, W. Zhang, Journal of colloid and interface science 509 (2018) 448-456.
[107] H. Wu, J. Ma, C. Zhang, H. He, Journal of Environmental Sciences 26 (2014) 673-682.
[108] D. Aphairaj, T. Wirunmongkol, S. Pavasupree, P. Limsuwan, Energy Procedia 9 (2011) 539-544.
[109] F. Jiang, S. Zheng, L. An, H. Chen, Applied Surface Science 258 (2012) 7188-7194.

[110] N.T. Hanh, N. Le Minh Tri, D. Van Thuan, M.H. Thanh Tung, T.-D. Pham, T.D. Minh, H.T. Trang, M.T. Binh, M.V. Nguyen, Journal of Photochemistry and Photobiology A: Chemistry 382 (2019).
[111] M.R. Delsouz Khaki, M.S. Shafeeyan, A.A.A. Raman, W.M.A.W. Daud, Journal of Molecular Liquids 258 (2018) 354-365.
[112] A.K. Benabbou, Z. Derriche, C. Felix, P. Lejeune, C. Guillard, Applied Catalysis B: Environmental 76 (2007) 257-263.
[113] H. Dong, G. Zeng, L. Tang, C. Fan, C. Zhang, X. He, Y. He, Water Research 79 (2015) 128-146.
[114] K. Nakata, A. Fujishima, Journal of Photochemistry and Photobiology C: Photochemistry Reviews 13 (2012) 169-189.
[115] K. Qi, B. Cheng, J. Yu, W. Ho, Journal of Alloys and Compounds 727 (2017) 792-820.
[116] R. Saravanan, V.K. Gupta, V. Narayanan, A. Stephen, Journal of Molecular Liquids 181 (2013) 133-141.
[117] S. Rehman, R. Ullah, A.M. Butt, N.D. Gohar, J Hazard Mater 170 (2009) 560-569.
[118] P.H. Le, L.T. Hieu, T.N. Lam, N.T.N. Hang, N.V. Truong, L.T.C. Tuyen, P.T. Phong, J. Leu, Micromachines (Basel) 9 (2018).
[119] G. Yang, Z. Jiang, H. Shi, T. Xiao, Z. Yan, Journal of Materials Chemistry 20 (2010) 5301-5309.
[120] M.-H. Hsu, C.-J. Chang, International Journal of Hydrogen Energy 39 (2014) 16524-16533.
[121] b. G. Poongodia, R. Mohan Kumarb,n, R. Jayavelc.
[122] O. Haibo, H.J. Feng, L. Cuiyan, C. Liyun, F. Jie, Materials Letters 111 (2013) 217-220.
[123] J. Shao, W. Sheng, M. Wang, S. Li, J. Chen, Y. Zhang, S. Cao, Applied Catalysis B: Environmental 209 (2017) 311-319.
[124] Y. Zhang, J. Chen, L. Hua, S. Li, X. Zhang, W. Sheng, S. Cao, Journal of Hazardous Materials 340 (2017) 309-318.
[125] Y. Zhang, Z. Zhao, J. Chen, L. Cheng, J. Chang, W. Sheng, C. Hu, S. Cao, Applied Catalysis B: Environmental 165 (2015) 715-722.
[126] D. Liu, R. Tian, J. Wang, E. Nie, X. Piao, X. Li, Z. Sun, Chemosphere 185 (2017) 574-581.
[127] A. Lisowska-Oleksiak, K. Szybowska, V. Jasulaitiené, Electrochimica Acta 55 (2010) 5881-5885.
[128] R. Mohan, K. Krishnamoorthy, S.-J. Kim, Solid State Communications 152 (2012) 375-380.
[129] H. Benhebal, M. Chaib, A. Leonard, S.D. Lambert, M. Crine, Materials Science in Semiconductor Processing 15 (2012) 264-269.
[130] B. Subash, B. Krishnakumar, R. Velmurugan, M. Swaminathan, M. Shanthi, Catalysis Science & Technology 2 (2012) 2319-2326.

[131] J.-C. Sin, S.-M. Lam, K.-T. Lee, A.R. Mohamed, Ceramics International 40 (2014) 5431-5440.
[132] S. Sharma, S. Mehta, S. Kansal, Journal of Alloys and Compounds 699 (2017) 323-333.
[133] S. Singhal, J. Kaur, T. Namgyal, R. Sharma, Physica B: Condensed Matter 407 (2012) 1223-1226.
[134] T.M. Hammad, J.K. Salem, R.G. Harrison, R. Hempelmann, N.K. Hejazy, Journal of Materials Science: Materials in Electronics 24 (2013) 2846-2852.
[135] M. Shirzad-Siboni, A. Jonidi-Jafari, M. Farzadkia, A. Esrafili, M. Gholami, Journal of Environmental Management 186 (2017) 1-11.
[136] U. Alam, A. Khan, D. Ali, D. Bahnemann, M. Muneer, RSC Advances 8 (2018) 17582-17594.
[137] A. Lavín, R. Sivasamy, E. Mosquera, M.J. Morel, Surfaces and Interfaces 17 (2019) 100367.
[138] A.V. Rane, K. Kanny, V.K. Abitha, S. Thomas, in: S. Mohan Bhagyaraj, O.S. Oluwafemi, N. Kalarikkal, S. Thomas (Eds.), Synthesis of Inorganic Nanomaterials, Woodhead Publishing, 2018, pp. 121-139.
[139] P. O'Brien, in: K.H.J. Buschow, R.W. Cahn, M.C. Flemings, B. Ilschner, E.J. Kramer, S. Mahajan, P. Veyssière (Eds.), Encyclopedia of Materials: Science and Technology, Elsevier, Oxford, 2001, pp. 1173-1176.
[140] B.G. Rao, D. Mukherjee, B.M. Reddy, in: D. Ficai, A.M. Grumezescu (Eds.), Nanostructures for Novel Therapy, Elsevier, 2017, pp. 1-36.
[141] T. Puntervold, A. Mamonov, Z. Aghaeifar, G.O. Frafjord, G.M. Moldestad, S. Strand, T. Austad, Energy & fuels 32 (2018) 7374-7382.
[142] M. El Ouahabi, L. Daoudi, N. Fagel, Clay Minerals 49 (2018) 35-51.
[143] L.D. M. El Ouahabi1*, F. De Vleeschouwer3,4, R. Bindler5, N. Fagel1.
[144] B.-L. Zhu, C.-L. Qi, Y.-H. Zhang, T. Bisson, Z. Xu, Y.-J. Fan, Z.-X. Sun, Applied Clay Science 179 (2019) 105138.
[145] C. Li, Z. Sun, X. Dong, S. Zheng, D.D. Dionysiou, Journal of Catalysis 367 (2018) 126-138.
[146] A.S. S. M. El-Sheikh*.
[147] C. Wang, H. Shi, P. Zhang, Y. Li, Applied Clay Science 53 (2011) 646-649.
[148] B. Sarkar, R. Rusmin, U.C. Ugochukwu, R. Mukhopadhyay, K.M. Manjaiah, Modified Clay and Zeolite Nanocomposite Materials, 2019, pp. 113-127.
[149] C. Belver, M.A. Bañares Muñoz, M.A. Vicente, Chemistry of Materials 14 (2002) 2033-2043.
[150] A. Tironi, M.A. Trezza, E.F. Irassar, A.N. Scian, Procedia Materials Science 1 (2012) 343-350.
[151] X. Xu, X. Lao, J. Wu, Y. Zhang, X. Xu, K. Li, Applied Clay Science 115 (2015) 76-86.
[152] J.d.S. Lopes, W.V. Rodrigues, V.V. Oliveira, A.d.N.S. Braga, R.T. da Silva, A.A.C. França, E.C. da Paz, J.A. Osajima, E.C. da Silva Filho, Applied Clay Science 168 (2019) 295-303.

[153] R. Patakfalvi, A. Oszkó, I. Dékány, Colloids and Surfaces A: Physicochemical and Engineering Aspects 220 (2003) 45-54.
[154] K. Dedkova, K. Matejova, J. Lang, P. Peikertova, K.M. Kutlakova, L. Neuwirthova, K. Frydrysek, J. Kukutschova, J Photochem Photobiol B 135 (2014) 17-22.
[155] K. Dedkova, B. Janikova, K. Matejova, P. Peikertova, L. Neuwirthova, J. Holesinsky, J. Kukutschova, J Photochem Photobiol B 148 (2015) 113-117.
[156] B. Janíková, J. Tokarský, K. Mamulová Kutláková, M. Kormunda, L. Neuwirthová, Applied Clay Science 143 (2017) 345-353.
[157] K. Mamulová Kutláková, J. Tokarský, P. Kovář, S. Vojtěšková, A. Kovářová, B. Smetana, J. Kukutschová, P. Čapková, V. Matějka, Journal of Hazardous Materials 188 (2011) 212-220.
[158] G.N. Shao, M. Engole, S.M. Imran, S.J. Jeon, H.T. Kim, Applied Surface Science 331 (2015) 98-107.
[159] L.V. Barbosa, L. Marçal, E.J. Nassar, P.S. Calefi, M.A. Vicente, R. Trujillano, V. Rives, A. Gil, S.A. Korili, K.J. Ciuffi, E.H. de Faria, Catalysis Today 246 (2015) 133-142.
[160] X. Li, H. Yang, Applied Clay Science 100 (2014) 43-49.
[161] C. Li, Z. Sun, W. Zhang, C. Yu, S. Zheng, Applied Catalysis B: Environmental 220 (2018) 272-282.
[162] H. Senoussi, H. Osmani, C. Courtois, M. el Hadi Bourahli, boletín de la sociedad española de cerámica y vidrio 55 (2016) 121-126.
[163] A. Shvarzman, K. Kovler, G.S. Grader, G.E. Shter, Cement and Concrete Research 33 (2003) 405-416.
[164] R. Fernandez, F. Martirena, K.L. Scrivener, Cement and Concrete Research 41 (2011) 113-122.
[165] C. Li, N. Zhu, X. Dong, X. Zhang, T. Chen, S. Zheng, Z. Sun, Advanced Powder Technology 31 (2020) 1241-1252.
[166] B.J. Saikia, G. Parthasarathy, J. Mod. Phys 1 (2010) 206-210.
[167] K. Lefatshe, C. Muiva, L. Kebaabetswe, Carbohydrate Polymers 164 (2017).
[168] K.G. Chandrappa, T.V. Venkatesha, K. Vathsala, C. Shivakumara, Journal of Nanoparticle Research 12 (2010) 2667-2678.
[169] X. Zhang, Y. Zhang, D. Wang, F. Qu, Journal of Nanomaterials 2014 (2014) 1-6.
[170] V. Wongso, C.J. Chen, A. Razzaq, N.A. Kamal, N.S. Sambudi, Applied Clay Science 180 (2019) 105158.
[171] C. Xu, L. Cao, G. Su, W. Liu, H. Liu, Y. Yu, X. Qu, Journal of hazardous materials 176 (2009) 807-813.
[172] Y. Wang, L. Liu, L. Xu, X. Cao, X. Li, Y. Huang, C. Meng, Z. Wang, W. Zhu, Nanoscale 6 (2014) 6790-6797.
[173] D. Wang, H. Shen, L. Guo, F. Fu, Y. Liang, New Journal of Chemistry 40 (2016) 8614-8624.

[174] O.A. Zelekew, D.-H. Kuo, J.M. Yassin, K.E. Ahmed, H. Abdullah, Applied Surface Science 410 (2017) 454-463.

[175] D. Ghosh, K. Bhattacharyya, Applied Clay Science 20 (2002) 295-300.

[176] K. Intarasuwan, P. Amornpitoksuk, S. Suwanboon, Advanced Powder Technology 24 (2013) 999-1005.

[177] C. Liu, D. Kong, P.C. Hsu, H. Yuan, H.W. Lee, Y. Liu, H. Wang, S. Wang, K. Yan, D. Lin, P.A. Maraccini, K.M. Parker, A.B. Boehm, Y. Cui, Nature Nanotechnology 11 (2016) 1098-1104.

[178] X. Jiang, Q. Lin, M. Zhang, G. He, Z. Sun, Nanoscale research letters 10 (2015) 30.

[179] P.A. Alaba, Y.M. Sani, W.M.A.W. Daud, RSC advances 5 (2015) 101127-101147.

[180] S. Sohrabnezhad, A. Pourahmad, M. Razavi, Applied Physics A 122 (2016) 822.

# APPENDIX I

Bandgap analysis for the selected catalyst

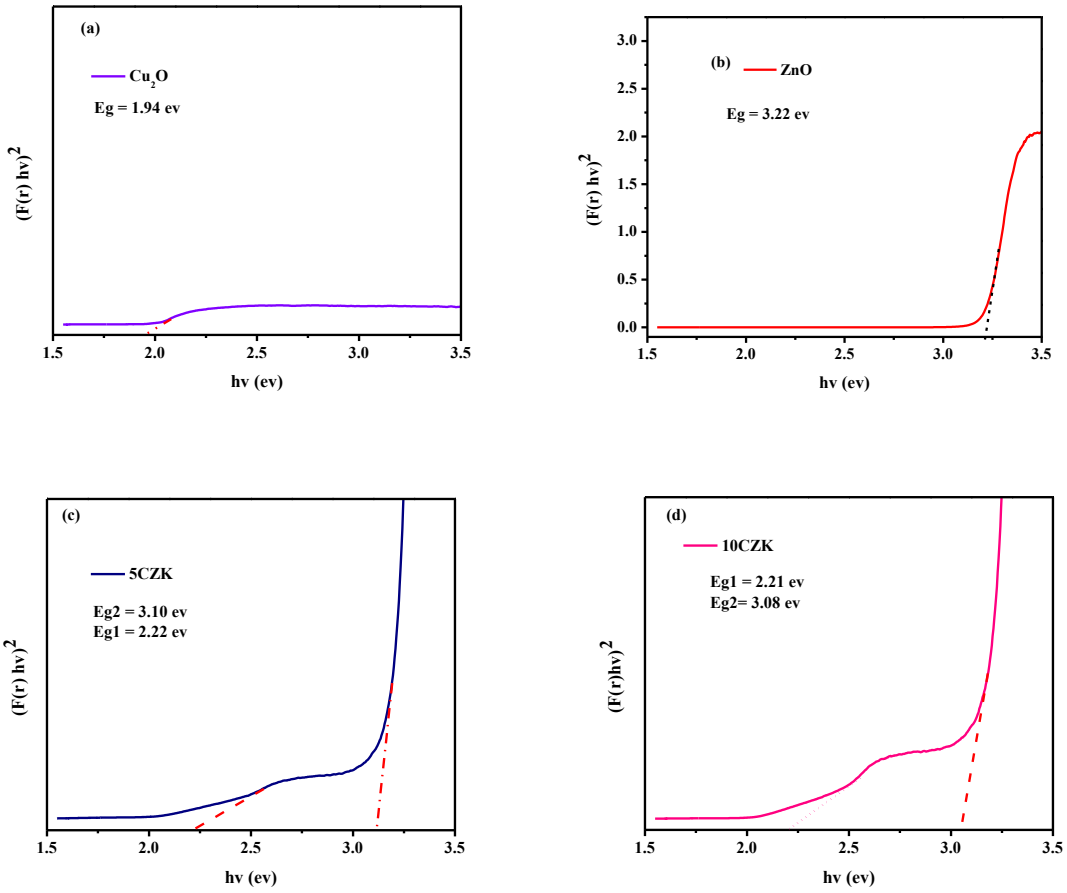

# APPENDIX II

Concentration changes with time for the selected catalyst